Section 2 Plasma Physics

Chapter 1. Plasma Dynamics

Academic and Research Staff

Professor George Bekefi, Professor Abraham Bers, Professor Bruno Coppi, Professor Jonathan S. Wurtele, Dr. Stefano Migliuolo, Dr. Abhay K. Ram, Dr. Barrett Rogers, Dr. Linda E. Sugiyama, Ivan Mastovsky

Visiting Scientists and Research Affiliates

Dr. Carson C. Chow,[1] Dr. Vladimir Fuchs,[2] Dr. Paolo Detragiache,[3] Dr. Marco Nassi,[3] Dr. Jiri Ullschmied,[4] Franco Carpignano,[5] George M. Svolos

Graduate Students

Neer R. Asherie, James C. Blastos, Palmyra E. Catravas, Kai P. Chan, Wen Hu, Alexander Matusis, Gregory E. Penn, Caterina Riconda, Todd H. Rider, Steven D. Schultz, Richard E. Stoner, Luigi Vacca, Pavel S. Volfbeyn

Undergraduate Students

Beth L. Chen, Jonathan C. Doan, David H. Hijirida, Hana Ohkawa, Kenneth N. Ricci

Technical and Support Staff

Felicia G. Brady, Laura B. Doughty, Catherine Lorusso, Laura M. von Bosau, Miriam Weiner

1.1 Relativistic Electron Beams

Sponsors

National Science Foundation
Grant ECS 89-02990
U.S. Air Force - Office of Scientific Research
Grant F49620-93-1-0108
U.S. Army - Harry Diamond Laboratories
Contract DAAL02-92-K-0037
U.S. Department of Energy
Grant DE-FG02-91ER-40648
U.S. Navy - Office of Naval Research
Grant N00014-90-J-4130

Project Staff

Professor George Bekefi, Professor Jonathan S. Wurtele, Dr. Jiri Ullschmied, Ivan Mastovsky, James C. Blastos, Palmyra E. Catravas, Beth L. Chen, Jonathan C. Doan, Wen Hu, Alexander Matusis, Kenneth N. Ricci, Richard E. Stoner, Pavel S. Volfbeyn

1.1.1 Observation of Frequency Chirping and Phase of a Free Electron Laser Amplifier

Temporal variations of frequency and phase are important parameters of pulsed free electron lasers (FEL) in many proposed applications such as, for example, in radar and communications and as drivers in novel high gradient accelerators. Such temporal variations (chirping) have been observed in wave propagation in passive media and can occur as a result of a time-dependent dielectric coefficient caused by changes in plasma density,[6] or as a result of a rapidly moving plasma-vacuum

---

1 University of Colorado, Boulder, Colorado.

2 Centre Canadien de Fusion Magnétique (CCFM), Quebec, Canada.

3 E.N.E.A., IEN "Galileo Ferraris", Turin, Italy.

4 Institute of Plasma Physics, Czech Academy of Sciences, P.O. Box 17, 182 00 Prague 8, Czech Republic.

5 A.S.P. Associazione per lo Sviluppo Scientifico e Tecnologico del Piemonte, Turin, Italy.

6 S.C. Wilks, J.M. Dawson, and W.B. Mori, "Frequency Up-Conversion of Electromagnetic Radiation with Use of an Overdense Plasma," *Phys. Rev. Lett.* 61: 337 (1989); C.J. Joshi, C.E. Clayton, K. Marsh, D.B. Hopkins, A. Sessler, and D. Whittum, "Demonstration of the Frequency Upshifting of Microwave Radiation by Rapid Plasma Creation," *IEEE Trans. Plasma Sci.* 18: 814 (1990); V.R. Goteti and D.K. Kalluri, "Wave Propagation in a Switched on Time Varying Plasma Medium," *IEEE Trans. Plasma Sci.* 17: 828

boundary.[7] In this paper, we report frequency and phase shift measurements in an active, lasing medium in which the wave amplitude exhibits exponential growth. Here, the time-varying dielectric medium represents the interaction between the pulsed relativistic electron beam of the free electron laser (FEL), the magnetic wiggler, and the copropagating electromagnetic wave launched into the system. The theoretical and computational modeling is described elsewhere.[8]

A schematic of the FEL[9] amplifier is shown in figure 1a. A mildly relativistic electron beam (750 keV) is generated by a Marx capacitor bank (Physics International Pulserad 110A). The electrons are emitted from a hemispherical graphite cathode by an explosive field-emission process. The graphite anode acts as an emittance selector, allowing only a small fraction of the essentially monoenergetic electron beam to propagate through its 2.54-mm radius and 62-mm-long aperture.

The 50-period bifilar helical wiggler produced by current-carrying helical wires has a period of 3.18 cm and provides a magnetic field of uniform amplitude whose magnitude on axis is adjustable up to 1.8 kG. The wiggler field intensity is slowly increased over the initial six periods, and provides an adiabatic input for the electron beam. The system, including the gun, is immersed in a uniform axial guide magnetic field generated by a solenoid. The intensity of this field can be varied up to a maximum of 11.6 kG.

The 2-m-long stainless-steel drift tube has an internal radius of 0.51 cm and acts as a cylindrical waveguide whose fundamental TE_{11} mode has a cutoff frequency of 17.2 GHz. The system is designed to operate in this lowest waveguide mode.

A high-power magnetron operating at 33.39 GHz is the input power source for the FEL amplifier. The wave launcher consists of a short section of circular waveguide of radius 0.31 cm into which ~ 12kW of power is coupled from a standard Ka-band rectangular waveguide. This section of circular waveguide supports only the fundamental TE_{11} mode for the operating frequency. Its radius is then adiabatically increased to the radius of the drift tube. A linearly polarized wave is thereby injected into the interaction region.

(1989); D.K. Kalluri, "Effect of Switching a Magnetoplasma Medium on a Traveling Wave: Longitudinal Propagation," *IEEE Trans. Antennas Propag.* 37: 1638 (1989).

7 W.B. Mori, "Generation of Tunable Radiation Using an Underdense Ionization Front," *Phys. Rev.* A44, 5118 (1991); P. Sprangle, E. Esarey, and A. Ting, "Nonlinear Interaction of Intense Laser Pulses in Plasmas," *Phys. Rev.* A41: 4463 (1990); H.C. Kapteyn and M.M. Murnane, "Relativistic Pulse Compression," *J. Opt. Soc. Am.* B8: 1657 (1991); R.L. Savage, Jr., W.B. Mori, C. Joshi, T.W. Johnston, and G. Shvets, "Tunable Radiation Generation Using Underdense Ionization," *Proceedings of the International Conference on Research Trends in Coherent Radiation Generation and Particle Accelerators,* LaJolla, California, February 11, 1992.

8 G. Shvets and J. Wurtele, "Frequency Shifting in Free-Electron Lasers," submitted to *Phys. Fluids.*

9 M.E. Conde and G. Bekefi, "Experimental Study of a 33.3-GHz Free-Electron-Laser Amplifier with a Reversed Axial Guide Magnetic Field," *Phys. Rev. Lett.* 67: 3082 (1991); M.E. Conde and G. Bekefi, "Amplification and Superradiant Emission from a 33.3 GHz Free Electron Laser with a Reversed Axial Guide Magnetic Field," *IEEE Trans. Plasma Sci.* 20: 240 (1992).

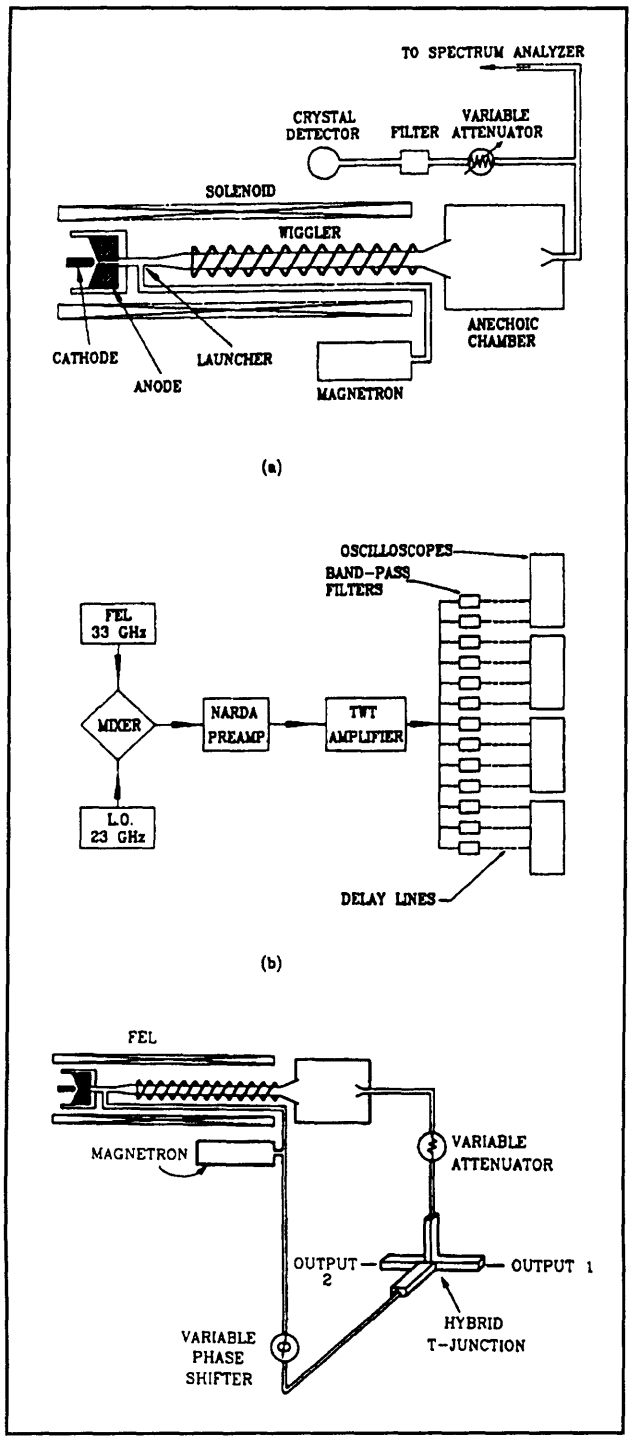

Figure 1. (a) Experimental arrangement of the FEL amplifier, (b) spectrum analyzer, and (c) interferometer.

The output power from the FEL is transmitted by means of a conical horn into a reflection free "anechoic chamber." A small fraction of the radiation is then collected by a receiving horn, passes through precision calibrated attenuators, and a 1.7-GHz-wide band-pass filter. The power levels are finally determined from the response of calibrated crystal detectors.

The radiation intensity, frequency and phase are measured as a function of interaction length within the wiggler. This length is varied by changing the distance that the electron beam is allowed to propagate in the drift tube. Application of a strong transverse magnetic field locally is sufficient to deflect the electrons into the waveguide wall and thereby terminate the interaction at that point.

All studies reported in this report were carried out in an FEL subjected to a combined axial magnetic field (B_z) and a helical wiggler field (B_w). The solid dots of figure 2 illustrate the optimal operational parameters in the three well known groups[9] indicated in the figure. Group I refers to the situation where the cyclotron wavelength $l_c \equiv 2\pi v_z \gamma m/eB_z$ in the guide field exceeds the wiggler wavelength l_w such that $l_c > l_w$. Group II corresponds to the case where the cyclotron wavelength is less than l_w, namely $l_c < l_w$; and the Reversed Field Regime is one in which the electron orbital motions in the guide and wiggler fields oppose one another ($-l_c < l_w$). The three operating regimes are separated by two singular, unstable regions. The one, referred to as gyroresonance, occurs where $l_c \sim l_w$; the other so called antiresonance occurs at $-l_c \sim l_w$.

Early studies of the frequency spectrum and chirping have been determined[10] by a heterodyne technique illustrated in figure 1b. A crystal rectifier was used as a mixer for the 33 GHz FEL radiation and for radiation from a variable frequency 23 GHz local oscillator. The resulting beat wave was amplified and sent to an array of band-pass waveguide filters. Thus, the calibrated response of the various channels provides, on a single shot basis, a direct histogram of output power in terms of radiation frequency.

The frequency spectra in the saturation region, corresponding to a measurement with a full length wiggler of ~ 180cm are shown in figure 3. We observe that in Group I the spectrum is shifted from the input magnetron frequency by ~ 100MHz. The 80 MHz width of each band-pass filter does not allow better resolution. Figure 3 also illustrates that, within the sensitivity of this technique, no fre-

[10] M.E. Conde, C.J. Taylor, and G. Bekefi, "Observations of Frequency Upshift in a Pulsed Free-Electron Laser Amplifier," *Phys. Fluids* B5: 1934 (1993).

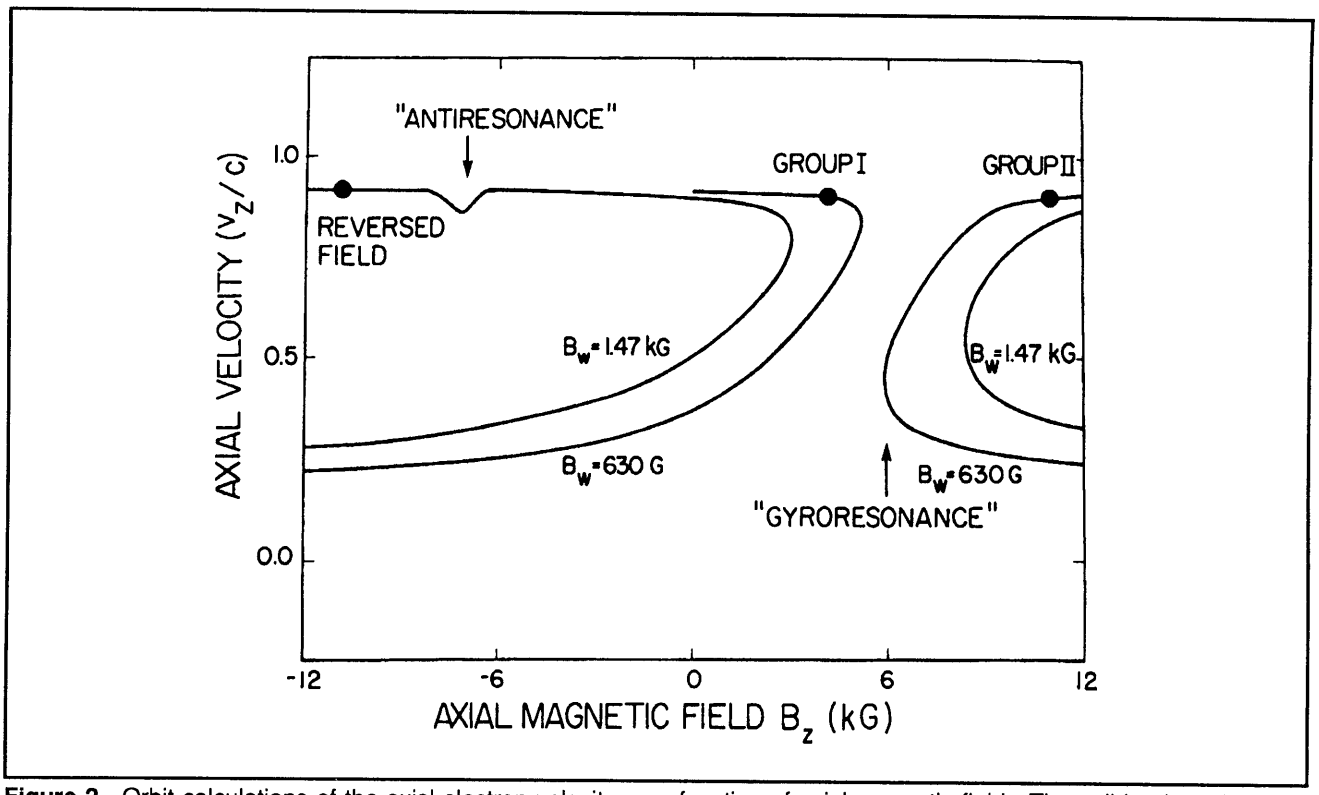

Figure 2. Orbit calculations of the axial electron velocity as a function of axial magnetic field. The solid points show the operating regimes at maximum measured RF output.

quency chirping is observed in either Group II or in the Reversed Field Regime.

In order to improve sensitivity and study frequency chirping (if any) in the two other FEL regimes, we resorted to the method shown in figure 1c. In this interferometric technique, the total phase difference between the reference and FEL input signals into the hybrid tee as a function of time t is found to be[11]

$$\cos\phi(t) = \frac{P_1(t) - P_2(t)}{2\sqrt{P_{FEL}(t)P_{REF}(t)}} \qquad (1)$$

Here $P_{FEL}(t)$ and $P_{REF}(t)$ are the instantaneous power inputs into the hybrid tee (see figure 1c) during the FEL voltage pulse; and $P_1(t)$ and $P_2(t)$ are the corresponding outputs from the tee. For every phase shifter setting ϕ_0, three shots are taken, and P_{FEL}, P_{REF}, P_1 and P_2 recorded. The phase shifter is then advanced by 60 degrees, and the procedure is repeated for a total of six successive settings of the phase shifter. A least squares algorithm then fits a sinusoid to the data recorded on the right hand side of Eq. 1 for all six phase shifter settings ϕ_0 (figure 4).

The procedure is repeated with the electron beam turned off, and a second sinusoid is generated. The phase slippage between the two sinusoids thereby derived then yields the desired phase change $\Delta\phi(t)$ caused by the FEL interaction.

Figure 5 illustrates the temporal behavior of the phase change $\Delta\phi(t)$ for a discrete set of time values chosen during the FEL pulse. The instantaneous frequency shift can then be obtained from the slope of these curves, namely $\Delta f = (1/2\pi)(d\Delta\phi(t)/dt)$. The large chirping observed in Group I and the relatively weak chirping in Group II and the Reversed Field Regime confirms the much cruder measurements depicted in figure 3. We note that Group I is characterized by strong frequency upshifts as well as downshifts, unlike Groups II and Reversed Field regimes where mostly upshifting is seen.

[11] T.J. Orzechowski, E.T. Scharlemann, and D.B. Hopkins, "Measurement of the Phase of the Electromagnetic Wave in a Free-Electron Laser Amplifier," *Phys. Rev.* A35: 2184 (1987).

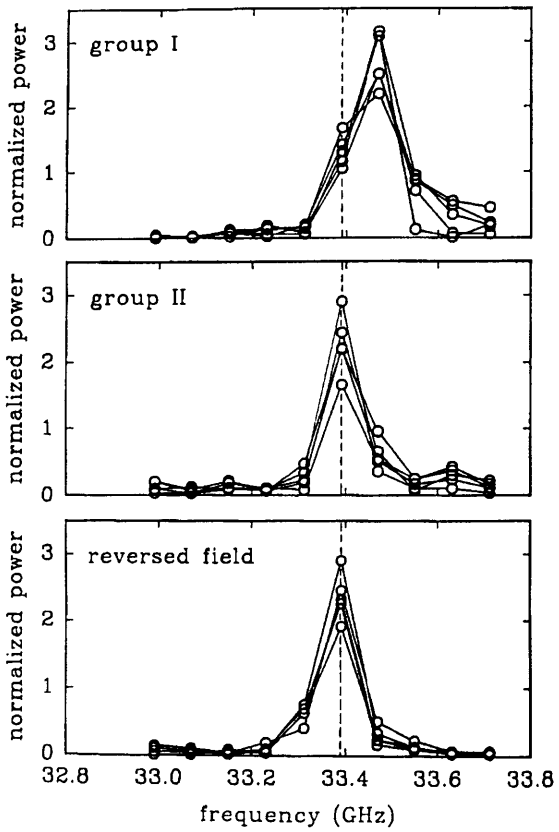

Figure 3. Frequency spectra for five successive shots.

The results shown in figure 5 were made for the full 180 cm interaction length z. Figure 6 illustrates how the magnitude of chirping varies with interaction length z. It is seen to be roughly linear with distance and remains so irrespective of whether the measurements are made in the small signal regime (z < 120cm) or in the nonlinear saturated regime (z > 120 cm).

Since the phase $\Delta\phi(t,z)$ has been measured at different times, t during the pulse and at different interaction lengths z, we can readily derive the phase shifts as function of z *averaged* over the duration of the pulse. The results are illustrated in figure 7 for the Reversed Field Regime, together with the corresponding power measurements. The curves represent simulations from the time independent WTDI code.[12]

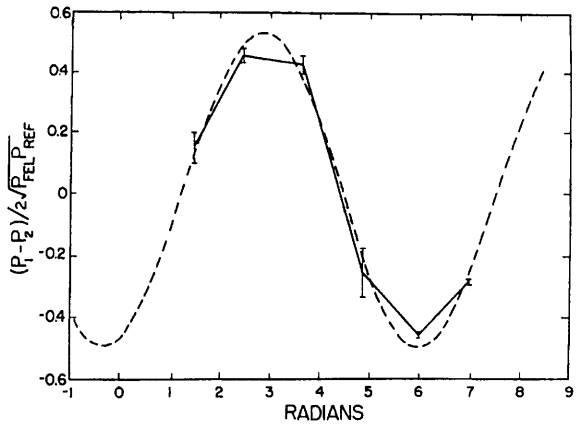

Figure 4. Typical sinusoidal curve fit to determine phase shift at a given time during the RF pulse.

In summary, we have carried out what we believe are the first spatio-temporal measurements of frequency $\Delta f(t,z)$ and phase $\Delta\phi(t,z)$ in a pulsed free electron laser amplifier. Such measurements can provide very sensitive tests of FEL theory. Moreover, they may also prove to be useful in future applications of free electron lasers in situations where very tight control of frequency and phase are demanded.

Erratic behavior of Δf may also be used as a signature of unstable FEL operation. To test this notion we have studied chirping at the "antiresonance" (see figure 2). Figure 8 (top) illustrates the lack of reproducibility of Δf on a series of successive shots. This is to be compared with the good reproducibility shown in figure 8 (bottom) taken in a FEL parameter range slightly removed from the precise position of the antiresonance. We note that such measurements are not possible at gyroresonance because here the instability is so strong that it drives the electrons into the waveguide walls.

[12] G. Zhang, G. Shvets, and J.S. Wurtele, "Theoretical Study of Free-Electron Lasers with Reversed Guide Field," *Nucl. Instr. Meth. Phys. Res.* A331: 472 (1993).

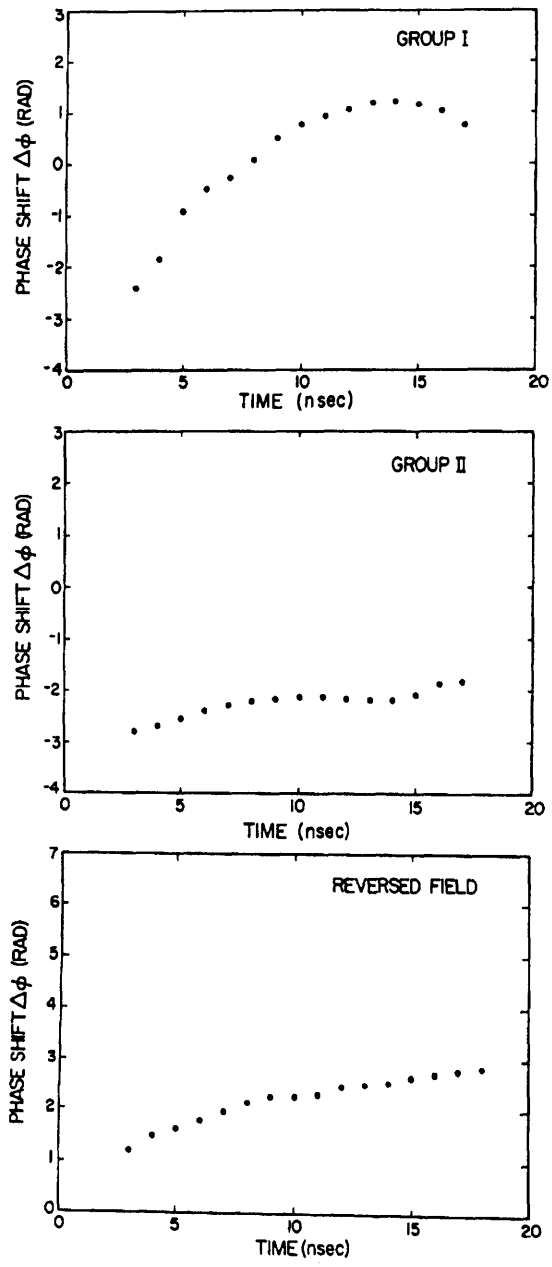

Figure 5. FEL phase shift at discrete times during the RF pulse (z = 180 cm).

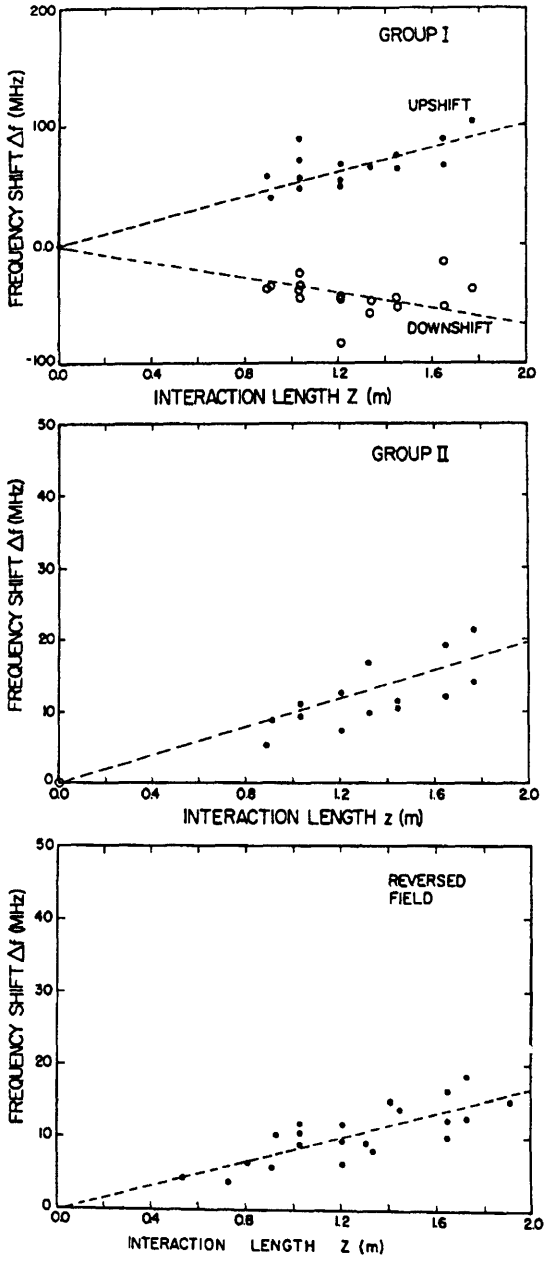

Figure 6. Frequency chirping as a function of interaction length. In Group I the maximum observed upshift, df/dz ≈ 50 MHz/mand downshift df/dz ≈ – 32 MHz/m. In Group II the upshift, time averaged over the pulse, df/dz ≈ 10 MHz/m. In the Reversed Field Regime the time average upshift df/dz ≈ 8 MHz/m.

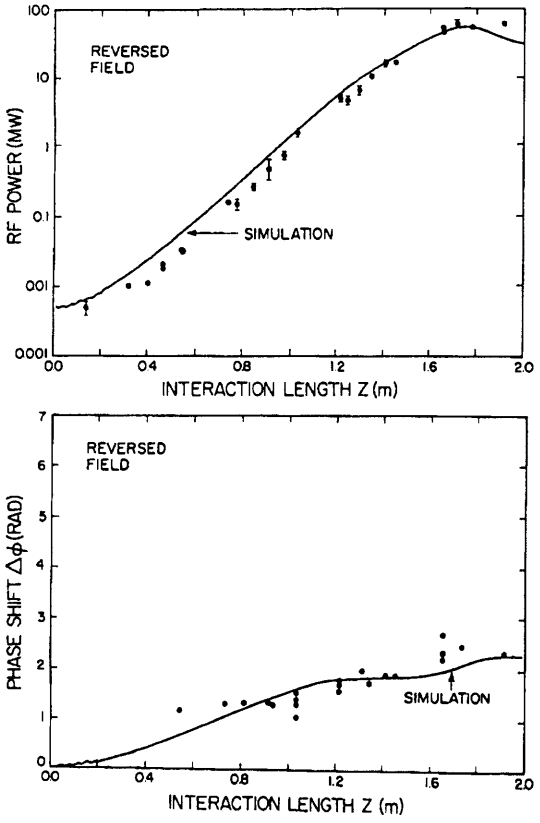

Figure 7. RF power and time averaged FEL phase change over the duration of the pulse as a function of interaction length, in the Reversed Field Regime.

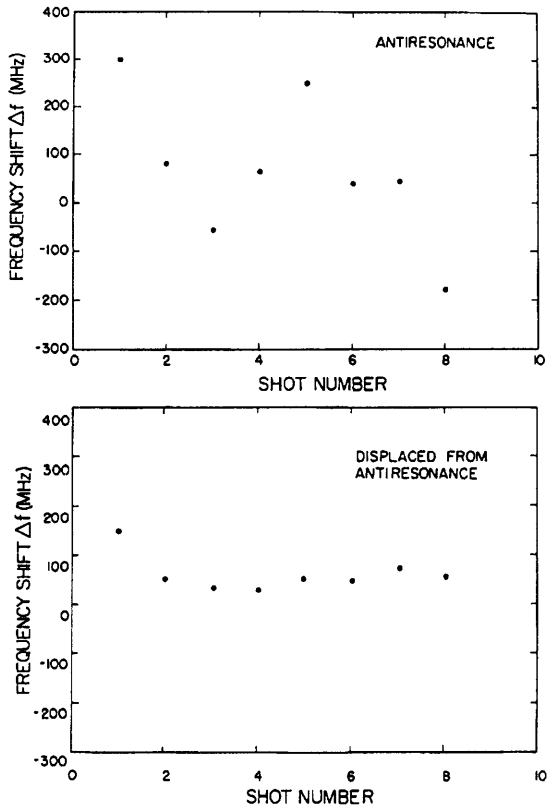

Figure 8. Chirping, showing erratic behavior at antiresonance ($B_z = -6.54$ kG) and consistent behavior slightly removed from antiresonance ($B_z = -7.36$ kG). See figure 2.

1.2 Plasma Wave Interactions—RF Heating and Current Generation

1.2.1 Introduction

Sponsors

National Aeronautics and Space Administration
Grant NAGW-2048
National Science Foundation
Grant ECS 88-22475
U.S. Department of Energy
Grant DE-FG02-91-ER-54109

Project Staff

Professor Abraham Bers, Dr. Abhay K. Ram, Dr. Carson C. Chow, Dr. Vladimir Fuchs, Kai P. Chan, Steven D. Schultz, Luigi Vacca

The research of this group is concerned with studies on the electrodynamics of plasmas. Attention is directed toward understanding the nonlinear dynamics of plasmas driven by high-frequency electromagnetic fields (as in RF heating and current drive of magnetically confined plasmas, or in laser-plasma interactions), and the generation and propagation of unstable radiations from laser-plasma interactions and anisotropic electron distributions in space and astrophysical plasmas.

In the following, we report on our continuing study of the synergistic enhancement of current drive efficiency with the use of multiple types of waves. We also report on further progress in understanding web-chaos induced by waves on ion-orbit dynamics that can lead to direct ion heating. The third report concerns further studies of an anomalous electron transport phenomenon we discovered a few years ago: stochastic streamers in electron guiding center dynamics interacting with electrostatic waves. The last report gives our initial results on arriving at a description of transport in intense ion-cyclotron heating of a high-temperature tokamak plasma.

1.2.2 Lower Hybrid Current Drive in the Presence of Waves in the Ion Cyclotron Range of Frequencies

Sponsor

U.S. Department of Energy
Grant DE-FG02-91-ER-54109

In the previous *RLE Progress Report*,[13] we discussed some recent experiments on the Joint European Tokamak (JET) where it was observed that the lower hybrid (LH) current drive (CD) efficiency was significantly enhanced when the lower hybrid current drive (LHCD) waves were launched in the presence of waves in the ion cyclotron range of frequncies (ICRF).

The initial ICRF power is carried from the antenna into the center of the plasma by fast Alfvén waves (FAW). Our previous calculations have shown that the FAW diffusion coefficient is very small compared to the LH diffusion coefficient so that the FAW could not significantly modify the electron distribution function and enhance the CD efficiency. However, the conditions for which the CD efficiency was observed to be enhanced allowed some of the input ICRF power to be mode converted to ion-Bernstein waves (IBW). The mode conversion occurs at ion resonance layers located inside the plasma and the IBWs then propagate away from these resonance layers towards the high magnetic field.[14] The mode conversion is most efficient for small $k_\parallel$'s ($k_\parallel$ is the component of the total wave vector along the toroidal magnetic field). The power mode converted to IBWs depends on the concentration of the minority ion species in a plasma. Mode conversion calculations[15] show that, for JET-type parameters with a hydrogen minority in a deuterium plasma, less than 25 percent of the incident FAW power, depending on the minority concentration $\eta = n_H/n_e$, is mode converted to IBWs:

Table 1. Mode conversion coefficient C versus η for $k_\parallel = 1\ m^{-1}$

η	0.1	0.05	0.03	0.01
C(%)	0.1	2.5	12	25

The mode conversion coefficient C decreases with increasing minority concentration η, with increasing $k_\parallel$, and with increasing minority temperature:

Table 2. C(%) as a function of minority temperature and $k_\parallel$ for $\eta = 0.02$

T_H (keV)	4	7	10	20
C ($k_\parallel = 1\ m^{-1}$)	13.4	10.8	8.8	4.5
C ($k_\parallel = 4\ m^{-1}$)	3.6	1.7	1.0	0.3

Since low $k_\parallel$s undergo mode conversion more effectively, a significant portion of the IBW power spectrum is at values of $v_\parallel$ that lie above the LH spectrum. The number of electrons resonant with these IBWs is negligibly small at such high parallel (to the total magnetic field) phase velocities of the waves. Thus, the IBWs cannot, initially, interact with the electron distribution function. The IBW spectrum also cannot interact with the ion distribution function as the mode conversion point is sufficiently far away from the ion cyclotron resonance. However, as the IBWs propagate away from the mode conversion region, toroidal effects upshift the $|k_\parallel|$'s so that eventually the IBW spectrum can interact with the electron distribution function and, in particular, with the energetic electron tail pulled out by the LHWs.

As shown in our previous RLE report,[16] the CD efficiency is determined by solving the Fokker-Planck equation for the flux-surface averaged electron distribution with the wave-electron interaction being described by the appropriate diffusion coefficient. For typical JET-type parameters, we find that:[17]

---

[13] *RLE Progress Report No. 135*, MIT, 1993, pp. 186-189.

[14] A.K. Ram and A. Bers, "Propagation and Damping of Mode-Converted Ion-Bernstein Waves in Toroidal Plasmas," *Phys. Fluids* B3: 1059 (1991).

[15] V. Fuchs and A. Bers, "Dissipative Mode Coupling in Ion-Cyclotron Resonance Minority Heating," *Phys. Fluids* 31: 3702 (1988).

[16] *RLE Progress Report No. 135*, MIT, 1993, pp. 186-189.

[17] A.K. Ram, A. Bers, and V. Fuchs, "Interaction of Ion-Bernstein Waves with Lower Hybrid Generated Suprathermal Electrons," *Bull. Am. Phys. Soc.* 38: 2108 (1993); A.K. Ram, A. Bers, and V. Fuchs, "Lower Hybrid Current Drive in the Presence of Ion Cyclotron Waves," *Proceedings of the 20th EPS Conference on Controlled Fusion and Plasma Physics*, Lisbon, Portugal, July 26-30, 1993, Vol. III, pp. 897-900; MIT Plasma Fusion Center Report PFC/JA-93-6, 1993; A.K. Ram, A. Bers, V. Fuchs, and R.W. Harvey, "Interaction of ICRF Waves with Lower Hybrid Driven Suprathermal Electrons," *Proceedings of the 10th Topical Conference on Radio*

$$\frac{D^{FAW}}{D^{LHW}} \sim \frac{1}{4}(k_{\perp}^{FAW}\rho_e)^2\left(\frac{v_{\perp}}{v_{\parallel}}\right)^2 \frac{\omega_{LHW}}{\omega_{ICRF}} << 1 \qquad (1)$$

where ρ_e is the electron Larmor radius. Equation (1) shows that the FAW diffusion coefficient is very small compared to the LHW diffusion coefficient. As pointed out before,[16] the FAW, due to its small diffusion coefficient, cannot by itself account for the enhancement in the CD efficiency.

The IBW diffusion coefficient does not lend itself to a simple analytical form. We can express the IBW diffusion coefficient[16] as $D^{IBW} = D_p^{IBW} D_\delta^{IBW}$ where D_δ^{IBW} is referred to as the "form factor." In figure 9, we show cD_δ^{IBW} (where c is the speed of light) as a function of the magnetic field. We find that D_δ^{IBW} increases with increasing magnetic field and, for a fixed magnetic field, D_δ^{IBW} decreases with the electron temperature. Thus, IBWs have to propagate away from the mode conversion region before the corresponding diffusion coefficient becomes large. Also, as the electron temperature increases, the IBWs have to propagate even farther in order to enhance the diffusion coefficient. Figure 10 shows the electron distribution function in the presence of LHWs alone and in combination with IBWs. For illustrative purposes, we have assumed that $D_p^{IBW}/(D_c v_e) = 20$ and $D_p^{LH}/(D_c v_e) = 10$ (v_e is the electron thermal velocity, $D_c = m_e^2 v_e^2 \nu$, m_e is the electron mass, and ν is the bulk electron-electron collision frequency). Figure 10 clearly shows that IBWs push electrons to higher momenta than for LWHs alone. In the case of LHWs alone, the calculated current drive efficiency is 0.39 A/W-m^2, while in the presence of IBWs, the current drive efficiency is found to increase to 0.52 A/W-m^2. Thus, IBWs can significantly stretch out the energetic electron distribution function and enhance CD efficiency.

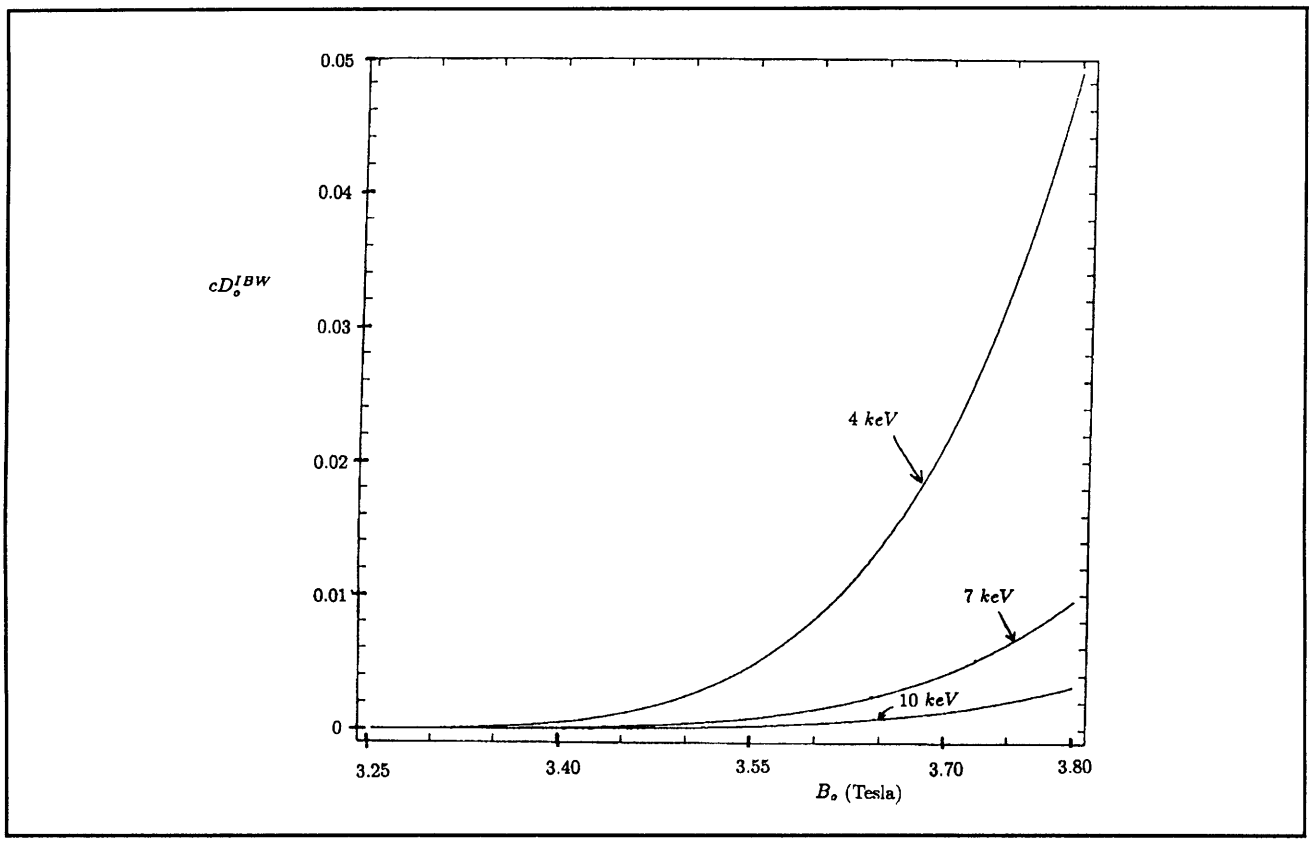

Figure 9. The IBW form factor (times the speed of light), cD_δ^{IBW}, as a function of the magnetic field, B_0. The curves are for three different plasma temperatures of 4, 7, and 10 keV. The plasma is a hydrogen minority in a deuterium plasma with $\eta = 0.03$. The electron density is 2×10^{13} cm^{-3}, $ck_\parallel/\omega_{ICRF} = 1.1$, and the ICRF frequency is 48 MHz. The form factor is shown for tail electrons with $p_\perp = 0$.

Frequency Power in Plasmas, Boston, Massachusetts, April 1-3, 1993, *A.I.P. Conf. Proc.* 289, eds. M. Porkolab and J. Hosea, (New York: American Institute of Physics, 1994), p. 293; MIT Plasma Fusion Center Report PFC/JA-93-4, 1993.

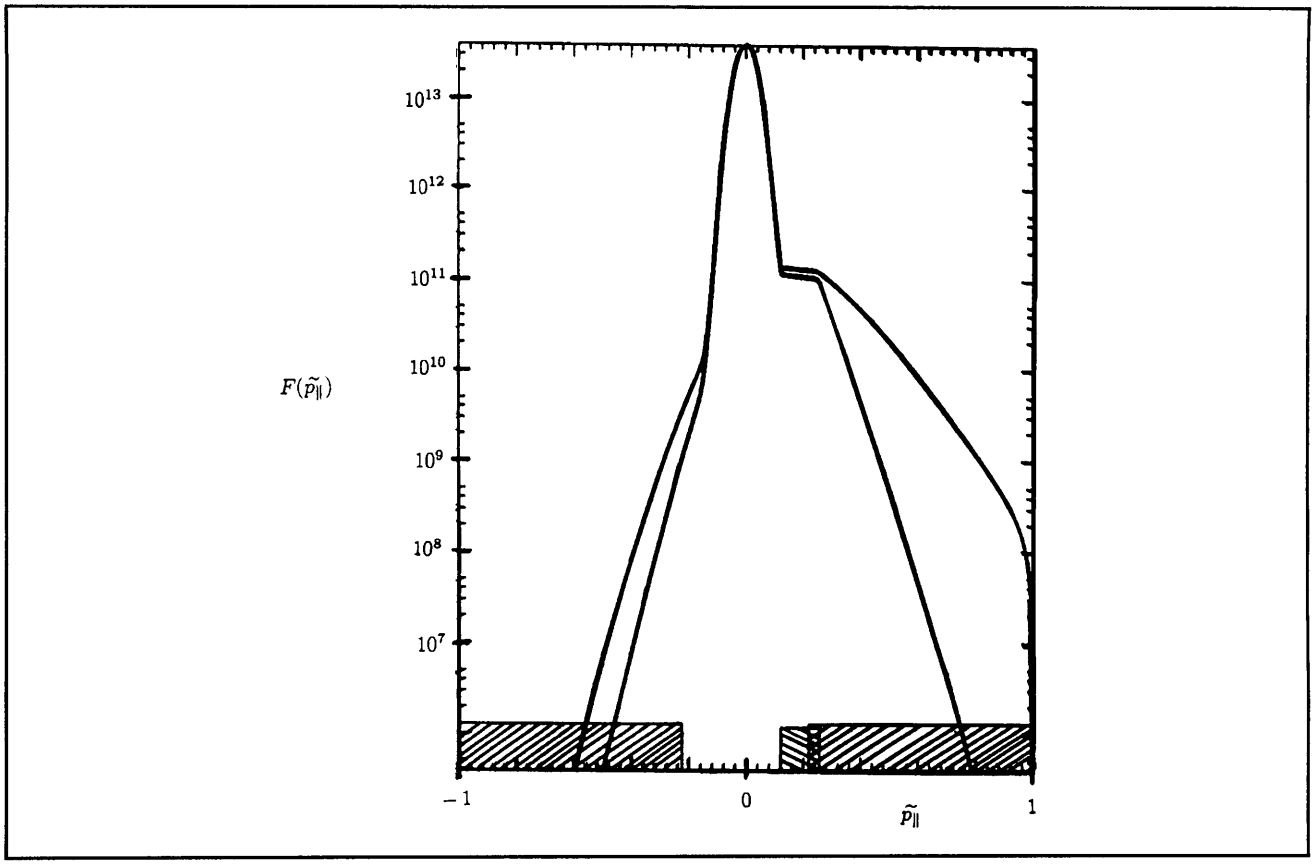

Figure 10. The parallel (to the magnetic field) electron distribution function versus normalized parallel momentum ($\tilde{p}_{\|}$). ($\tilde{p}_{\|} = 1$ corresponds to an electron energy of 1 MeV.) The plasma is a hydrogen minority in a deuterium plasma with η = 0.03. The electron density is 2 × 10^{13} cm^{-3}, the magnetic field is 3.7 Tesla, the temperature of the electrons and ions is 4 keV, the LHW frequency is 3.7 GHz, and the ICRF frequency is 48 MHz. The small dashed box (with the right inclined lines) is the parallel momentum extent of the LHW spectrum while the two larger dashed boxes (with the left inclined lines) give the parallel momentum extent of the IBW spectrum. The IBW spectrum is symmetric because the launched ICRF spectrum is symmetric in $k_{\|}$. The narrow (in $\tilde{p}_{\|}$) inside curve is the distribution function due to LHWs only; while the broader outside curve is due to the combination of LHWs and IBWs.

In our previous calculations, we have estimated D_p^{IBW} for the IBW in a very approximate way. In order to explain the JET results, we need a good estimate of D_p^{IBW}. For this, we have begun to do ray tracing of the IBWs[18] in order to determine the flux-surface averaged diffusion coefficient along the rays.

1.2.3 Fixed Points in Near Resonance Chaotic Webs

Sponsor

National Science Foundation
Grant ECS 88-22475

This is a continuing study on which we first reported in last year's *RLE Progress Report No. 135* (pp. 184-186). Its aim is to arrive at understanding wave induced chaos in ion dynamics in a magnetic field. The electrostatic wave is assumed to propagate across the magnetic field, and its frequency can be either very near an ion-cyclotron harmonic or in-between two ion-cyclotron harmonics. The basic equations were given in last year's report.

[18] A.K. Ram and A. Bers, *Phys. Fluids* B3: 1059 (1991).

Here, we report on the motion of first-order fixed points as the frequency is changing from on resonance to off resonance.

We isolate the m-th harmonic term from the Hamiltionian to obtain $H = \tilde{H}_0 + \alpha\tilde{H}_1$, where

$$\tilde{H}_0(\tilde{I}, \phi) = (\tilde{\omega}_0 m-1)\tilde{I} + \alpha J_m\left(\sqrt{\frac{2m\tilde{I}}{\tilde{\omega}_0}}\right)\cos\phi \qquad (1)$$

and

$$\tilde{H}_1 = \sum_{n=-\infty;\, n\neq m}^{\infty} J_n\left(\sqrt{\frac{2I}{\tilde{\omega}_0}}\right)\cos(n\psi-\tau) \qquad (2)$$

Corresponding to (1), the equations of motion are:

$$\frac{d\tilde{I}}{d\tau} = -\frac{\partial\tilde{H}_0}{\partial\phi} = \alpha J_m\left(\sqrt{\frac{2m\tilde{I}}{\tilde{\omega}_0}}\right)\sin\phi \qquad (3)$$

$$\frac{d\phi}{d\tau} = \frac{\partial\tilde{H}_0}{\partial\tilde{I}} =$$

$$(\tilde{\omega}_0 m-1)+\alpha\sqrt{\frac{m}{2\tilde{\omega}_0\tilde{I}}}\,J'_m\left(\sqrt{\frac{2m\tilde{I}}{\tilde{\omega}_0}}\right)\cos\phi$$

The positions of the first order islands and separatrices are given by the elliptic and hyberbolic fixed points, respectively. To solve for the fixed points, we set both $\frac{d\tilde{I}}{d\tau}$ and $\frac{d\phi}{d\tau}$ to zero. After rearranging terms, we find

$$\sin\phi J_m\left(\sqrt{\frac{2m\tilde{I}}{\tilde{\omega}_0}}\right) = 0 \qquad (4)$$

$$\cos\phi J'_m\left(\sqrt{\frac{2m\tilde{I}}{\tilde{\omega}_0}}\right) = \frac{(1-\tilde{\omega}_0 m)}{\alpha}\sqrt{\frac{2\tilde{\omega}_0\tilde{I}}{m}} \qquad (5)$$

The set of elliptic fixed points are given by $\sin\phi = 0$ and hyperbolic fixed points by $J_m\left(\sqrt{\frac{2m\tilde{I}}{\tilde{\omega}_0}}\right) = 0$. When we are exactly on resonance, we have $\tilde{\omega}_0 m = 1$ and the RHS of equation (5) becomes zero. The elliptic fixed points and the hyperbolic fixed points form a checkered pattern, shown in figure 11.

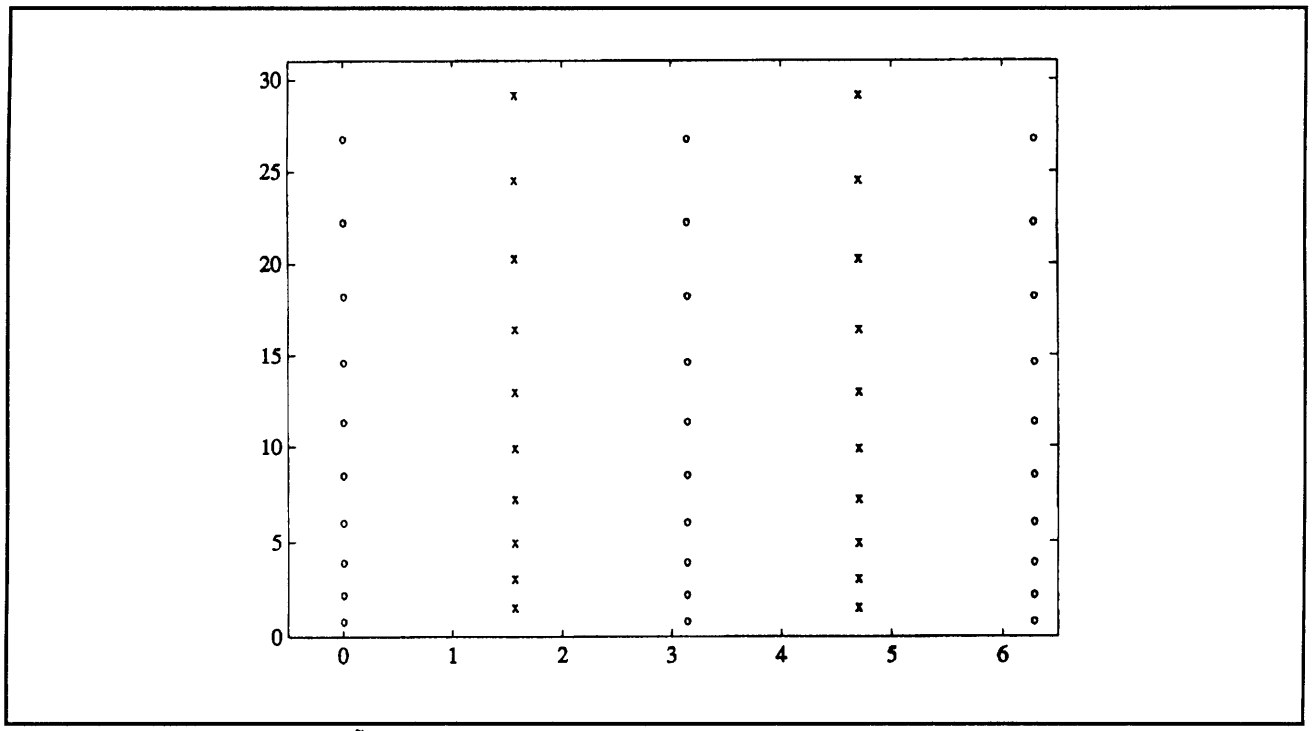

Figure 11. Fixed points with $1/\tilde{\omega}_0 = 5$, $\alpha = 0.01$. x - hyperbolic fixed points; o - elliptic fixed points.

When $1/\tilde{\omega}_0$ moves away from resonance, say $1/\tilde{\omega}_0 = m+\delta$ (δ small), the elliptic fixed points move in a vertical path, and the hyperbolic fixed points move in a roughly horizontal path. The result of this movement is that pairs of elliptic points and pairs of hyperbolic points group together into clusters of four. As $1/\tilde{\omega}_0$ departs more and more from resonance, the two pairs of fixed points get closer together until they meet and annihilate each other. Fixed points with large $\tilde{I}$ move faster and are annihilated sooner. This is illustrated in figure 12.

The Hamiltonian $\tilde{H}_0(\tilde{I}, \phi)$ does not display chaos. Instead chaos arises from the perturbation $\alpha\tilde{H}_1(I, \psi, \tau)$. Our interest is in the evolution of chaos along the web when α, the magnitude of the wave, increases. However, when increasing α, we not only change the width of the web, but also change the position of the fixed points. Since the fixed points define the position of the primary islands and separatrices, changing them will also change the separatrices along which the web evolves. Hence it becomes difficult to study the effects of $\alpha\tilde{H}_1(I, \psi, \tau)$ because they are obscured by changes in $\tilde{H}_0(\tilde{I}, \phi)$ (compare figure 13 with figure 14).

To remedy this difficulty, we notice from the RHS of equation (5) that the positions of fixed points depend on the parameter:

$$\eta = \frac{(1-\tilde{\omega}_0 m)}{\alpha}\sqrt{\frac{\tilde{\omega}_0}{m}} \propto \frac{\delta}{\alpha} \qquad (6)$$

Hence when we increase α, we can also increase δ to keep η constant and thereby keep the fixed points in place. This will minimize (although not eliminate) the changes in $\tilde{H}_0(\tilde{I}, \phi)$ so that the onset of chaos due to the perturbation will be more evident (compare figure 13 with figure 15). Work along these lines is continuing.

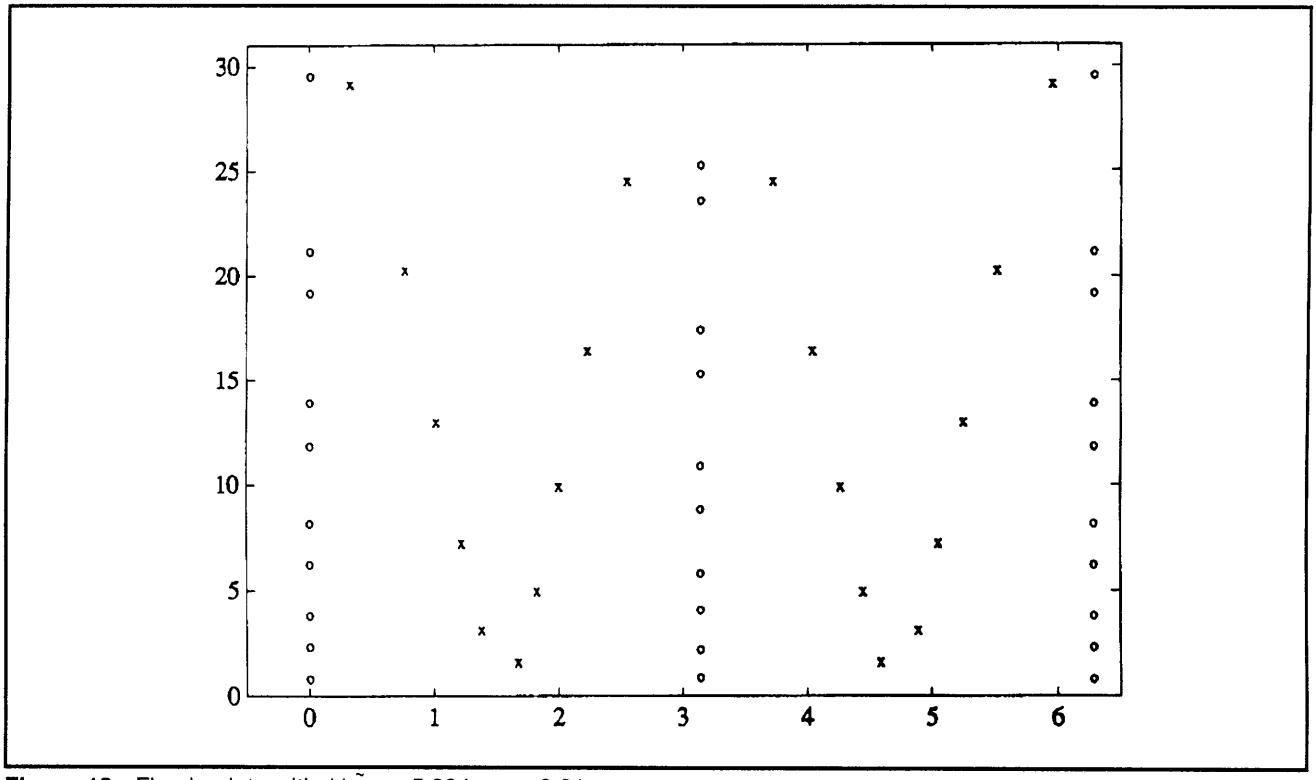

Figure 12. Fixed points with $1/\tilde{\omega}_0 = 5.004$, $\alpha = 0.01$.

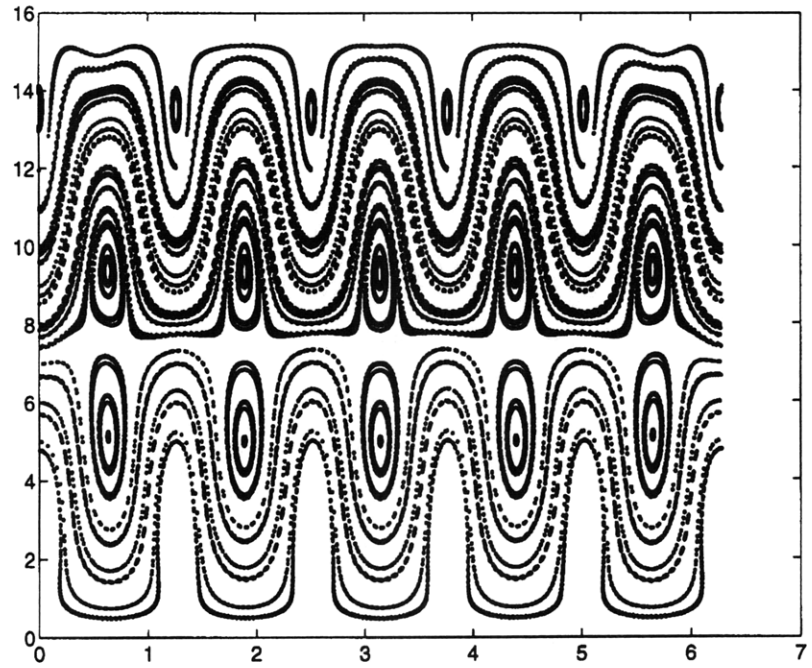

Figure 13. Particle orbits (I against ψ) with $1/\tilde{\omega}_0 = 5.02$, $\alpha = 0.01$.

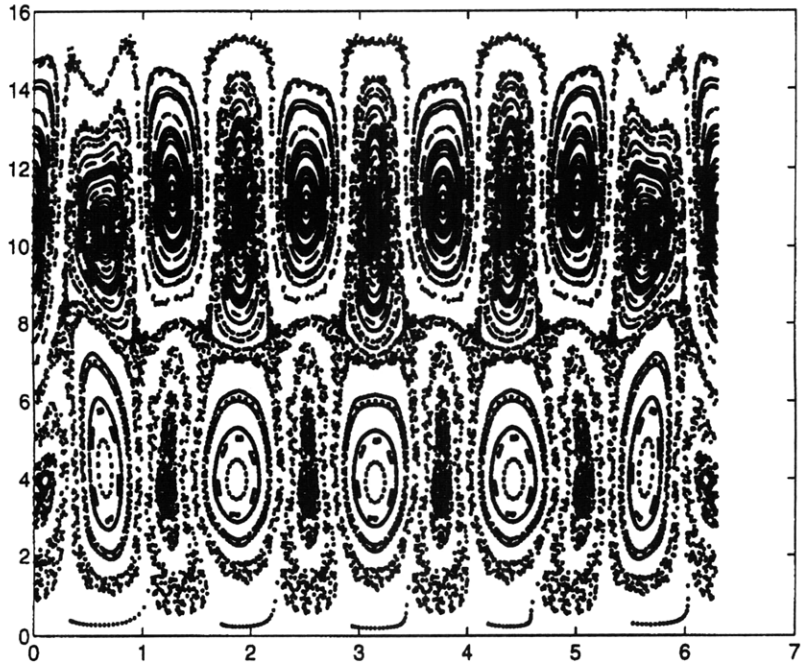

Figure 14. Particle orbits (I against ψ) with $1/\tilde{\omega}_0 = 5.02$, $\alpha = 0.05$.

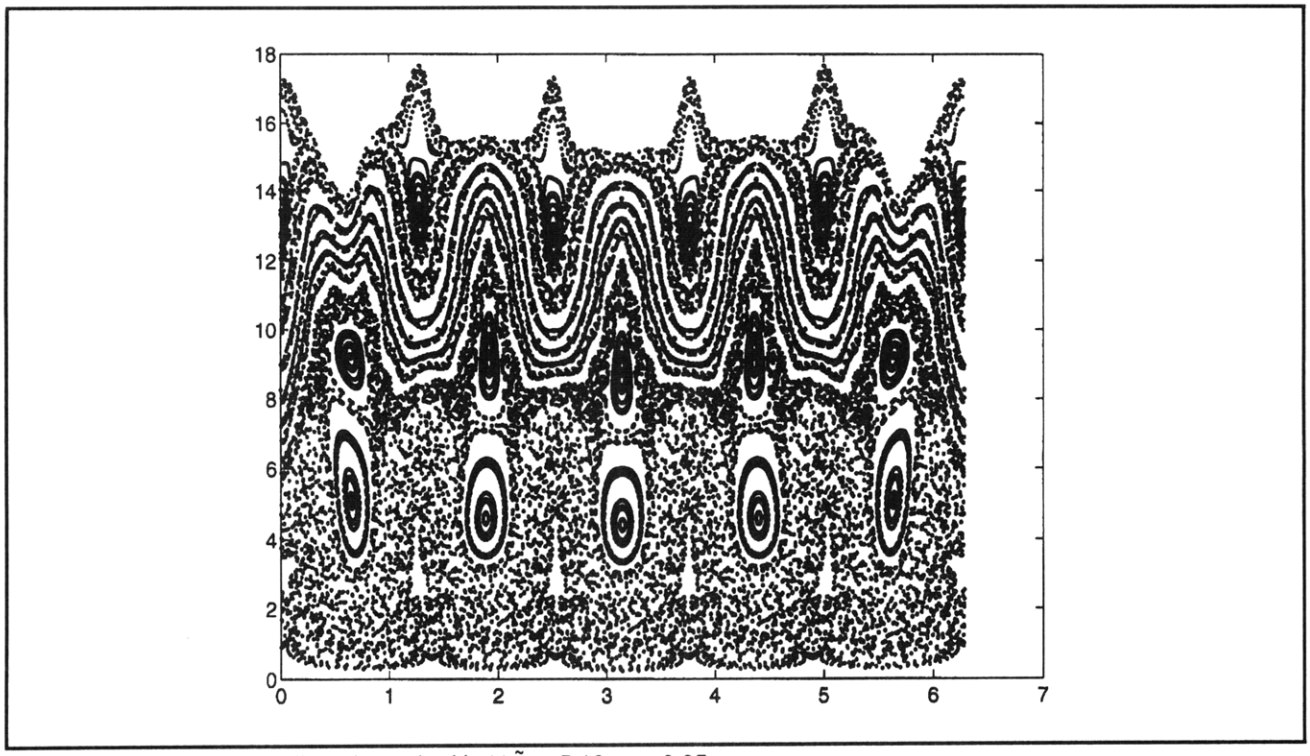

Figure 15. Particle orbits (I against ψ) with $1/\tilde{\omega}_0 = 5.10$, $\alpha = 0.05$.

1.2.4 Anomalous Electron Guiding Center Streaming Due to Waves

Sponsors

Magnetic Fusion Science Fellowship Program
National Science Foundation
Grant ECS 88-22475
U.S. Department of Energy
Grant DE-FG02-91-ER-54109

The motion of circulating electrons in a tokamak interacting with a discrete spectrum of waves is given by a Hamiltonian formuation in the guiding center limit and studied by numerical integration.

Recent work by Kupfer[19] on the chaotic electron dynamics induced by electrostatic waves demonstrated that an electron, on a flux surface with rational safety factor q, which is in resonance with two waves with identical parallel phase velocity can have a "streaming" motion perpendicular to the magnetic field. Theoretical analysis of this problem is complicated by the necessity of visualizing dynamics in a four-dimensional phase space including both parallel and radial motion.

We use a Hamiltonian description of the electron guiding center motion[20] that was derived by making use of several previous guiding center theories.[21] The model is based on a tokamak with an MHD equilibrium in the low-beta limit, and a low inverse-aspect ratio $\varepsilon = r/R$. The electron is assumed circulating, with an orbit which remains near its initial flux surface. A small magnetic field shear can also be included in this tokamak geometry. The phase space for the guiding center motion is reduced to four dimensions by gyroaveraging and by assuming that the magnetic moment μ is a constant: this requires that our study be restricted to waves in the low-frequency, long-wavelength limit. The derivation gives two sets of canonical coordinates for the

---

19 K. Kupfer, A. Bers, and A.K. Ram, in "Research Trends in Physics: Nonlinear and Relativistic Effects in Plasmas," ed. V. Stefan, (New York: Amer. Inst. of Phys., 1992), pp. 670-715; K. Kupfer, *Dynamical Chaos and Transport Induced by Waves in Plasmas*, Ph.D. diss., Dept. Nuc. Eng., MIT, 1991.

20 K. Kupfer, *Dynamical Chaos and Transport Induced by Waves in Plasmas*, Ph.D. diss., Dept. Nuc. Eng., MIT, 1991.

21 R.G. Littlejohn, "Variational Principles of Guiding Centre Motion," *J. Plasma Phys.* 29: 111 (1983); J.R. Cary and R.G. Littlejohn, "Noncanonical Hamiltonian Mechanics and Its Application to Magnetic Field Line Flow," *Annals of Physics* 151(1): 1 (1983); J.D. Meiss and R.D. Hazeltine, "Canonical Coordinates for Guiding Center Particles," *Phys. Fluids B* 2: 2563 (1990).

guiding center, (z_1, p_1) and (z_2, p_2). In terms of the familiar guiding center position (ψ, θ, ϕ) and parallel velocity $v_{||}$, and omitting correction terms of order ε, we find:

$$z_1 \sim \phi \qquad p_1 \sim mR_0 v_{||}$$

$$z_2 \sim \phi - q_0\theta \qquad p_2 \sim e\psi \tag{1}$$

Here q_0 is the safety factor. The Hamiltonian in the absence of wave perturbations is

$$H_0 = \frac{1}{2m_e R_0^2}\left[p_1^2 + \frac{s_0}{e} p_1 p_2^2\right] + \mu B_0. \tag{2}$$

Here we have included shear in the form of $s_0 = \frac{1}{q_0}\frac{\partial q_0}{\partial \psi}$, which is assumed to be small.

Drifts are accounted for in the order-ε corrections of (z_1, p_1, z_2, p_2), which are not given here.

The simplest perturbation to this Hamiltonian is an electrostatic field, in the form of a few discrete plane waves with identical frequency, whose potential is given by:

$$\Phi = \sum_{n,m} \Phi_{nm} \cos(n\phi + m\theta + k_\psi \psi - \omega t) \tag{3}$$

where n and m are mode numbers. For a given frequency, k_ψ is found using the dispersion relation, e.g., appropriate to lower-hybrid waves. Using the approximate relations given in equation (1), we obtain

$$\Phi = \sum_{n,m} \Phi_{nm} \cos(k_1 z_1 + k_2 z_2 + k_\psi p_2 - \omega t) \tag{4}$$

with $k_1 = n + (m/q_0)$ and $k_2 = -(m/q_0)$. The dynamics of interest occur when the safety factor q_0 is a rational number, which makes the perturbation periodic in z_1 and z_2 and allows us to choose different integers n,m giving the same value of the parallel mode number k_1 but different values of k_2 and k_ψ.

The electron is in resonance with a wave when $d(k_1 z_1 + k_2 z_2 + k_\psi p_2 - \omega t)/dt = 0$. The unperturbed Hamiltonian gives $\dot{z}_1 \sim (m_e R_0^2)^{-1} p_1$ and the other three coordinates constant, so resonance occurs for $p_1 \sim (m_e R_0^2)(\omega/k_1)$.

The equations of motion derived from the perturbed Hamiltonian were used to numerically integrate the motion $z_1(t)$, $p_1(t)$, $z_2(t)$, $p_2(t)$. We select units so that m_e, e, R_0, and ω are all unity. The safety factor is chosen to be $q_0 = 2$. To reproduce the radial streaming observed by Kupfer,[22] we choose four electrostatic modes with mode numbers (n,m) = (1,1)(1,2)(2,0)(2,2); in the new coordinates (k_1, k_2) = (3/2,-1/2)(2,-1)(2,0)(3,-1). This case is degenerate: two modes have the same parallel mode number $k_1 = 2$ with different values of k_2 and k_ψ. The resonance condition in simplified units is $p_1 = 1/k_1$, so that the resonance surfaces in phase space are at p_1 = 2/3, 1/2, and 1/3. The amplitude of each wave is the same and was chosen so that the separatrix layers for these three waves barely overlap, which creates a stochastic layer around all three of the resonance surfaces in (z_1, p_1) phase space. The initial condition of the coordinates is chosen to lie in this resonance region. The figures describe the motion observed for two cases with different initial conditions in (z_2, p_2). The two points are started on the same flux surface (p_{20}=0) but at different poloidal angles separated by $\Delta\theta = \pi/2$ ($z_{20} = 0, \pi$).

Figure 16 shows the time series $p_1(t)$ (which corresponds to parallel velocity) for these two cases. In the $z_{20} = 0$ case, p_1 is observed to fluctuate rapidly throughout the resonance region, spending a roughly equal amount of time near each of the three resonances. However, in the $z_{20} = \pi$ case, the electron quickly moves into an orbit close to the $p_1 = 1/2$ resonance, which is degenerate, and stays there. Figure 17 shows the time series $p_2(t)$ (corresponding to the flux coordinate) in the two cases. In the first case, motion in the p_2 direction is wildly fluctuating, but with occasional periods of directed, non-chaotic motion. Over long times, these periods of streaming add up to a slow drift in the radial direction. In the second case, this streaming motion is nearly continuous, and the rapid fluctuations are no longer visible on this scale, which is more than an order of magnitude larger than on the previous figure.

---

22 K. Kupfer, *Dynamical Chaos and Transport Induced by Waves in Plasmas*, Ph.D. diss., Dept. Nuc. Eng., MIT, 1991.

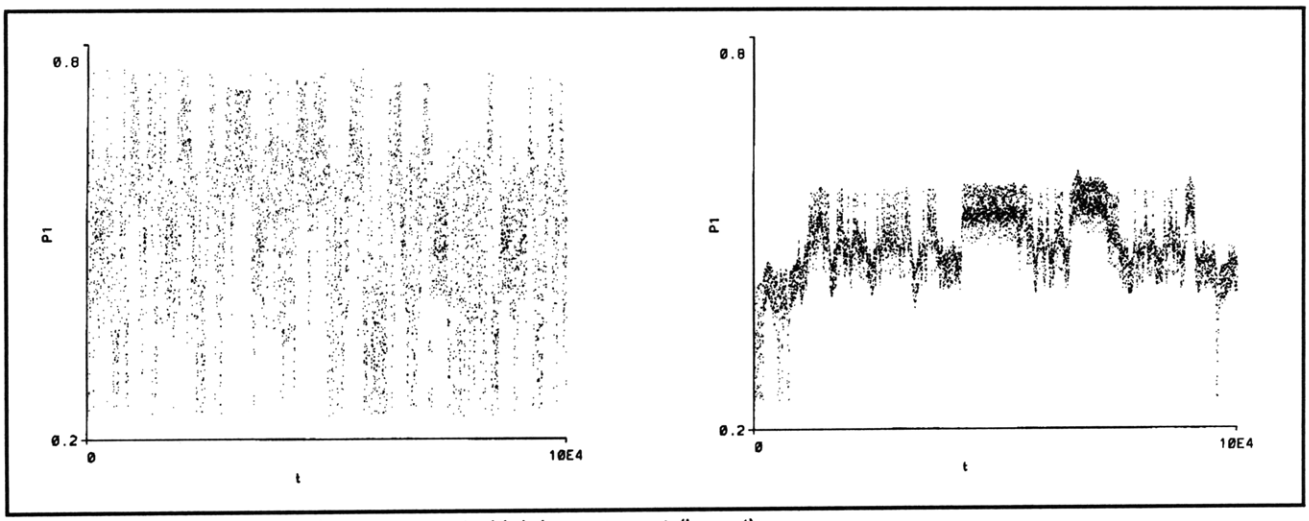

Figure 16. (left) p_1 versus t (in ω^{-1}); $z_{20} = 0$. (right) p_1 versus t (in ω^{-1}); $z_{20} = \pi$.

The electron streaming appears to be related to the patterns of constructive and destructive interference of the two degenerate waves. Let us explicitly add two such waves:

$$\Phi_0 \cos(k_1 z_1 + k_{2a} z_2 + k_{\psi a} p_2 - t)$$

$$+ \Phi_0 \cos(k_1 z_1 + k_{2b} z_2 + k_{\psi b} p_2 - t) \qquad (5)$$

$$= 2\Phi_0 \cos(\Delta k_2 z_2 + \Delta k_\psi p_2) \cos(k_1 z_1 + \bar{k}_2 z_2 + \bar{k}_\psi p_2 - t),$$

where $\bar{k}_2 = (k_{2a} + k_{2b})/2$, $\Delta k_2 = (k_{2a} - k_{2b})/2$, $\bar{k}_\psi = (k_{\psi a} + k_{\psi b})/2$, and $\Delta k_\psi = (k_{\psi a} - k_{\psi b})/2$. It is easy to show with equation (5) that $z_{20} = \pi$, $p_{20} = 0$ is a point where the degenerate waves interfere destructively. For an electron at this point, the $k_1 = 2$ waves appear to vanish, and the regions of phase space affected by the remaining waves no longer overlap.

We would like to see how this interference pattern affects the phase space of the guiding center motion. Unfortunately, a surface of section in this phase space is given by a four-dimensional mapping, which is impossible to visualize. But if a canonical transformation can be found so that two of the four phase space variables are nearly constants of the motion, a plot of this mapping in the phase plane of the other two coordinates is an approximate surface of section. The details of the canonical transformation giving this approximate surface of section are under investigation. This is expected to reveal that there are quantities which are very nearly conserved by the streaming motion.

We are currently working on a similar phase-space analysis of electron guiding center motion in electromagnetic waves, for example fast Alfvén waves. This problem is complicated by the fact that the canonical phase-space coordinates are shifted when a magnetic potential is added to this analysis.

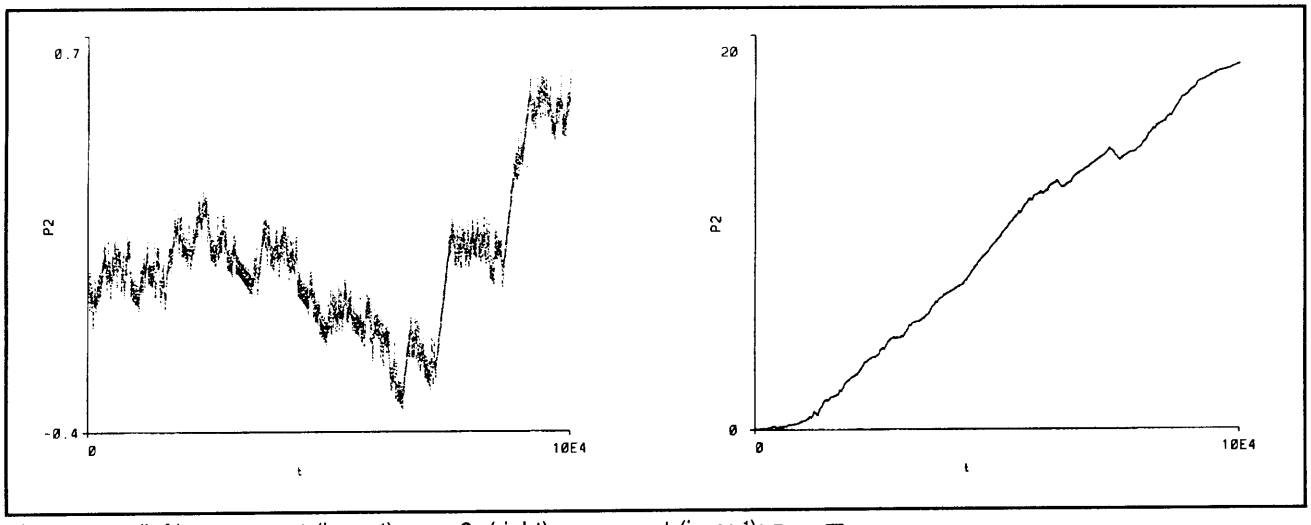

Figure 17. (left) p_2 versus t (in ω^{-1}); $z_{20} = 0$. (right) p_2 versus t (in ω^{-1}); $z_{20} = \pi$.

1.2.5 Resonant Fast Alfvén Wave-Particle Interaction in a Tokamak

Sponsor

U.S. Department of Energy
Grant DE-FG02-91-ER-54109

Ion heating in a tokamak by fast Alfvén wave fields has been the subject of numerous investigations both analytical and numerical. In particular, these studies have led to a description of the ion distribution function in the presence of such fields by Fokker-Planck equations in velocity space.[23] However, such Fokker-Planck equations do not include the induced transport due to the fields. For intense heating of tokamak plasmas, it is important to evaluate the spatial transport that may accompany such heating. We have initiated such a study.

Several simplifying assumptions are usually made in order to describe the field-induced diffusion in velocity space. The most serious ones are the neglect of finite banana widths and spatial diffusion induced directly by the wave. Changes in parallel velocity due to Doppler-shifted cyclotron resonances are responsible for spatial transport due to fields. This is immediately seen for trapped particles once one considers the change in toroidal angular momentum due to parallel velocity changes. This effect is mostly relevant at the magnetic axis of a tokamak. In order to study these effects one has to estimate the changes in space and velocity that an ion undergoes through resonance.

We have studied resonance interactions using Hamiltonian formalism in a perturbative way.[24] We assume a small wave amplitude with respect to the equilibrium field; this allows us to write a Hamiltonian of the following form:

$$H \simeq H_0 + \lambda H_1 \tag{1}$$

where λ is a parameter that accounts for the smallness of the wave amplitude. The leading order Hamiltonian is the usual guiding center Hamiltonian:

$$H_0 = \frac{1}{2} m v_{\|}^2 + \mu B \tag{2}$$

The wave-particle resonance is contained in H_1. The perturbed Hamiltonian is Fourier-decomposed as follows:

$$H_1 = \sum_k H_{1k} e^{i\psi(k)} \tag{3}$$

where

$$\psi_1(k) = N\zeta + M\theta - k_\perp r - \omega t + \phi + \alpha + \pi/2 \tag{4}$$

---

23 G. Kerbel and M. McCoy, "Kinetic Theory and Simulation of Multispecies Plasmas in Tokamaks Excited with Electromagnetic Waves in the Ion-Cyclotron Range of Frequencies," *Phys. Fluids* 28: 3629 (1985); P.J. Catto and J.R. Myra, "A Quasilinear Description for Fast-Wave Minority Heating Permitting OFF-Magnetic Axis Heating in a Tokamak," *Phys. Fluids B* 4: 187 (1992).

24 C. Grebogi, A.N. Kaufman, and R. Littlejohn, "Hamiltonian Theory of Ponderomotive Effects of an Electromagnetic Wave in a Non-Uniform Magnetic Field," *Phys. Rev. Lett.* 43: 1668 (1979).

and

$$H_{1k} = \frac{iq}{2\omega}\sqrt{2B\mu/m}\,[J_0 e^{-i\alpha}E_{+k}+J_2 e^{i\alpha}E_{-k}] \quad (5)$$

The equations of motion due only to wave interaction in a tokamak with circular flux surfaces, where the unit vector in the direction of the magnetic field is given by $b(r) = f(r)e_\zeta + g(r)e_\theta$, are:

$$\dot{X}_{gc_1} \simeq \sum_k \frac{1}{qB^*} b \times \nabla\psi_1(k)H_{1k}e^{i\psi(k)} \quad (6)$$

$$\dot{\mu}_1 = -\sum_k \frac{iq}{m} H_{1k}e^{i\psi(k)} \quad (7)$$

$$\dot{\phi}_{gc_1} = \sum_k \frac{q}{m}\frac{\partial H_{1k}}{\partial \mu} e^{i\psi(k)} \quad (8)$$

$$\dot{v}_{\|_1} \simeq -\sum_k \frac{B^*}{mB^*} \cdot \nabla\psi_1(k)H_{1k}e^{i\psi(k)} \quad (9)$$

The wave-particle interaction is localized in space so that the change in the guiding center variables can be evaluated by integrating equations (6) - (9) in the vicinity of the resonance region. Outside this region, the particle is essentially unperturbed by the wave. The wave-particle resonance condition is given by: $d\psi_1(k)/dt = 0$. Thus, the change in guiding center variables is:

$$\Delta A = \int_{res}\sum_k \hat{A}_{1k}e^{i\psi_1(k)}dt \quad (10)$$

where A represents any guiding center phase variable. Using the stationary phase approximation:

$$\Delta A \simeq \sum_k \hat{A}_{1k}|_{res}\int_{res} e^{i\psi_1(k)}dt \quad (11)$$

We now need to solve for the phase integral in the resonance region.

We introduce the resonance integral defined as

$$I = \int_{res} e^{i\psi} =$$

$$t_b\sum_{M,N}\int_{res} e^{-i[\omega_{tb}\hat{t}-\phi-N\zeta-M\theta+\alpha]}\frac{d\hat{t}}{d\theta}d\theta \quad (12)$$

where this integral has to be evaluated along the unperturbed orbit in the resonance region. Here α is held to be a constant and $\hat{t} = t/t_b$, $\omega_{tb} = \omega t_b$, where $t_b = R_0/v_{th}$.

Resonance integrals for passing particles were evaluated in two simple cases: without Doppler-shift and with Doppler-shift for an asymmetric monochromatic wave. For a resonance without Doppler-shift the resonant point is given by the coordinates that satisfy $\omega = qB/m$.

The resonant integral at leading order is easily evaluated:

$$\frac{I}{t_b} \simeq \sqrt{\frac{2\pi}{\omega_{c0}t_b}}\left(\frac{e^{-i\psi}}{\sqrt{gv_{\|th}\sin\theta}}\right)_{res} e^{\pm i\pi/4} \quad (13)$$

When we include the Doppler-shift for a monochromatic wave we obtain for the resonance condition:

$$\left(\frac{d\psi}{d\theta}\right)_{res} \simeq$$

$$(\omega_{tb}-\omega_{cb})\frac{1}{v_{\|th}}\frac{a}{R_0}\frac{x}{g} - M - N\frac{f}{gh}\frac{a}{R_0}x = 0 \quad (14)$$

where $h = 1+\frac{r}{R_0}\cos\theta$ and $x = r/a$. The resonance integral can be evaluated asymptotically:

$$\frac{I}{t_b} \simeq \left[\frac{a}{R_0}\frac{x}{g}\frac{1}{v_{\|th}}e^{-i\psi}\right]_{res}\sqrt{\frac{2\pi}{|\psi''_{res}|}}e^{\mp i\pi/4} \quad (15)$$

where

$$\frac{d^2\psi}{d\theta^2} \simeq \quad (16)$$

$$-x^2\sin\theta\left(\frac{a}{R_0}\right)^2\left[\frac{\omega_{cob}}{fg}\frac{1}{v_{\|th}}+\frac{\omega_{cob}}{hgf^2}\frac{\hat{\mu}}{2v^3_{\|th}}+N\frac{f}{g}\right]$$

Future work will include the evaluation of resonance integrals for trapped particles and the extension to multichromatic spectra.

1.2.6 Publications

Chow, C.C., and A. Bers. "Chaotic Stimulated Brillouin Scattering in a Finite Length Medium." *Phys. Rev. A* 47: 5144 (1993).

Chow, C.C., A. Bers, and A.K. Ram. "Spatiotemporal Chaos in the Nonlinear Three-Wave Interaction." In *Research Trends in Physics: Chaotic Dynamics and Transport in Fluids and Plasmas.* Eds. I. Prigogine, W. Horton, Y. Ichikawa, and G. Zaslavsky. New York: American Institute of Physics, 1993, pp. 305-322.

Ram, A.K., and A. Bers. "Hamiltonian Chaos in Wave-Particle Interactions." Invited paper presented at the 1993 Cambridge Workshop on Theoretical Geoplasma Physics. *Physics of Space Plasmas.* Forthcoming.

Ram, A.K., A. Bers, and V. Fuchs. "Lower Hybrid Current Drive in the Presence of ICRF Waves." Proceedings of the International Sherwood Fusion Theory Conference, Newport, Rhode Island, March 29-31, 1993.

Ram, A.K., A. Bers, and V. Fuchs. "Lower Hybrid Current Drive in the Presence of Ion Cyclotron Waves." Cambridge: MIT Plasma Fusion Center Report PFC/JA-93-6, May 1993.

Ram, A.K., A. Bers, and V. Fuchs. "Lower Hybrid Current Drive in the Presence of Ion Cyclotron Waves." *Proceedings of the 20th European Physical Society Conference on Controlled Fusion and Plasma Physics*, Lisbon, Portugal, July 26-30 1993. Eds. J. Costa Cabral, M.E. Manso, F.M. Serra, and F.C. Schüller. Part III, pp. 897-900.

Ram, A.K., A. Bers, V. Fuchs, and R.W. Harvey. "Interactions of ICRF Waves with Lower Hybrid Driven Suprathermal Electrons." *Proceedings of the Tenth Topical Conference on Radio Frequency Power in Plasmas*, April 1-3, 1993. Ed. M. Porkolab. New York: American Institute of Physics. Forthcoming.

Ram, A.K., A. Bers, V. Fuchs, and R.W. Harvey. "Interactions of ICRF Waves with Lower Hybrid Driven Suprathermal Electrons." Cambridge: MIT Plasma Fusion Center Report PFC/JA-93-4, April 1993.

Schultz, S.D., A. Bers, and A.K. Ram. "Anomalous Electron Streaming Due to Waves in Tokamak Plasmas." *Proceedings of the Tenth Topical Conference on Radio Frequency Power in Plasmas*, April 1-3, 1993. Ed. M. Porkolab. New York: American Institute of Physics. Forthcoming.

Schultz, S.D., A. Bers, and A.K. Ram. "Anomalous Electron Streaming Due to Waves in Tokamak Plasmas." Cambridge: MIT Plasma Fusion Center Report PFC/JA-93-5, April 1993.

Tao, Z.C., A.K. Ram, A. Bers, and G. Kalman. "Space-Time Evolution of Beam-Plasma Instability in Strongly Correlated Plasmas." *Phys. Rev. E* 48: R676 (1993).

Tao, Z.C., A.K. Ram, A. Bers, and G. Kalman. "Space-Time Evolution of Beam-Plasma Instability in Strongly Correlated Plasmas." Cambridge: MIT Plasma Fusion Center Report PFC/JA-93-7, May 1993.

1.3 Physics of Thermonuclear Plasmas

Sponsor

U.S. Department of Energy
Contract DE-FGO2-91ER-54109

Project Staff

Professor Bruno Coppi, Neer R. Asherie, Franco Carpignano, Dr. Paolo Detragiache, David H. Hijirida, Dr. Stefano Migliuolo, Dr. Marco Nassi, Hana Ohkawa, Gregory E. Penn, Caterina Riconda, Todd H. Rider, Dr. Barrett Rogers, Dr. Linda E. Sugiyama, George M. Svolos

As our primary activity in this research program, we study the theory of magnetically confined plasmas in regimes relevant to present-day advanced experiments and to future thermonuclear devices. In the future, these devices will probably ignite the plasma ("thermonuclear fuel") within toroidal magnetic confinement configurations and will involve either first generation fuels, a deuterium-tritium mixture (Ignitor, ITER), or more advanced fuels such as deuterium-deuterium or deuterium-helium mixtures (Candor).

The Ignitor-Ult machine is now in the early stages of construction in Europe. At MIT, the Alcator C-MOD experiment has recently begun operation. Alcator C-MOD combines the favorable features of an elongated plasma cross section with a high magnetic field to produce high plasma currents. This machine is in fact very similar to Megator, an experiment we proposed in the early 1970s as a logical continuation of the Alcator program.

Currently, our research program follows two major avenues. First, we are studying the basic physical

processes of thermonuclear plasmas (equilibrium, stability, transport, etc.) as they apply to existing or near-term future systems. In this effort, we closely collaborate with our experimental colleagues and with theorists from other research groups (e.g., Columbia University, JET, Phillips Laboratory, Princeton University, University of Texas, Lawrence Livermore National Laboratories). This work also involves time-dependent simulations of plasma discharges in the Ignitor-Ult experiment. We focus particular attention on the evolution of spatial profiles of plasma current and temperature. Collaboration with our colleagues at the Ente per le Nuove technologie l'Energia e l'Ambiente (E.N.E.A.) in Italy, as well as inhouse code development, plays a major role in this endeavor.

Second, we explore advanced regimes of thermonuclear burning, including those employing low neutron yield fuels (D-^{3}He, and "catalyzed" D-D). We consider both the design of machines that will contain these very high temperature plasmas as well as the physics that govern their behavior. Below, we discuss some of the salient results of work completed or presently being carried out by members of our research group.

1.3.1 Hyper-Cyclotron Emission (HCE) Induced by Fusion Reaction Products

We have proposed a theoretical interpretation and developed the relevant analysis for the radiation emission above the cyclotron frequency of the fusion products that has been observed in well confined plasma experiments[25] with a significant population of fusion reaction products. The emission spectrum typically shows distinct peaks at multiples (p=1 to 7 in the case of the Deuterium-Tritium plasma experiments carried out by the JET machine) of the alpha particle cyclotron frequency Ω_α. The frequency values suggest that the emission is coming from a localized region at the outer edge of the plasma column. For $p \geq 8$, the spectrum becomes continuous, while below $\omega = \Omega_\alpha$ some smaller peaks are observed. We have found that by considering the interaction of radially localized compressional Alfvén modes with anisotropic (in velocity space) alpha particle distributions, we can explain the key features of the discrete part of the spectrum. The continuum component of the spectrum is related to the presence of magnetic shear and to the transition from compressional Alfvén modes to whistler modes that occurs as the ratio ω/Ω_α increases. It is the overlapping of a class of these quasi-whistler modes that is proposed to produce the continuum.

We have investigated the radial structure of the Alfvén mode in detail. We find it to be localized in the plasma at a radius which agrees with the experiment results (for the discrete component of the spectrum) obtained by the JET machine.[26] Since we are assuming the plasma to be cold, we use the MHD equations with the addition of the Hall term in Ohm's law to study the mode structure in this frequency range. This work has been performed in a cylindrical geometry,[27] and will be extended to the toroidal case in order to fully understand the poloidal structure of the mode.

The calculation of the mode structure has been carried out assuming that plasma is composed of deuterium and tritium. This brings out the essential features of the problem, but neglects the effects of impurity ions. As the impurities are typically much heavier than the bulk plasma ions, they introduce resonances for $\omega < \Omega_D$ (the cyclotron frequency of deuterium = Ω_D) which may correspond to the smaller peaks measured experimentally. In addition, they introduce a significant correction to the Alfvén speed.[28]

We have explored some of the aspects related to the linear growth rate, γ_α, of the HCE instability. In particular, it is the perpendicular velocity gradient,[29] $\partial f_\alpha/\partial v_\perp$, that determines whether the mode is unstable or not. Throughout this work it has been assumed that the background plasma is cold. Although this is a good assumption for the electrons, complications arise for the ions. Energy is transferred from the alpha particles to the mode

---

[25] JET Team, "Fusion Energy Production from a Deuterium-Tritium Plasma in the JET Tokamak," *Nucl. Fusion* 32: 187 (1992).

[26] B. Coppi, "Origin of Radiation Emission Induced by Fusion Reaction Products," *Phys. Lett. A* 172: 439 (1993).

[27] N. Asherie, B. Coppi and C. Riconda, "Spatial Structure of Ion Cyclotron Frequency Modes Driven by Fusion Reactions," *Bull. Am. Phys. Soc.* 38: 2055 (1993).

[28] N. Asherie and B. Coppi, "Theoretical Analysis of the Emissions at the Cyclotron Frequency Harmonics of Fusion Produced Alpha Particles," *Proceedings of the Sherwood Fusion Theory Conference*, 1993, paper 1C19.

[29] B. Coppi and N. Asherie, "Theoretical Predictions and Experimental Evidence for Emission at the Cyclotron Frequency Harmonics of Fusion Produced α-Particles," *Bull. Am. Phys. Soc.* 37: 1475 (1992).

which then transfers its energy to the ions. Eventually the ions have enough energy so that thermal corrections (e.g., resonance broadening) become important. This may affect the growth rate in a significant way.[30]

1.3.2 Stabilization of External MHD Instabilities

An obstacle to reaching the second stability region[31] in toroidal magnetic confinement experiments is the possible onset of ideal MHD external modes driven predominantly by the current density gradient near the edge of the plasma column. This region in parameter space is one where the plasma is stable against pressure gradient driven internal MHD instabilities, while having a relatively high value of $\beta_p = 8\pi p/B_\theta^2$. A recent series of analyses[32] have shown that these regimes correspond to equilibria with plasma currents that are peaked toward the outer edge of the torus and can excite macroscopic external modes.

By considering a simple cylindrical equilibrium with magnetic field $B(r) = \hat{e}_z B_z + \hat{e}_\theta B_\theta$ and $\beta = 8\pi p/B^2 \circ \ominus 1$, $B_\theta/B_z \sim a/R \circ \ominus 1$ we begin to explore the possible self-healing of the plasma by diamagnetic effects. Since the external modes tend to have toroidal mode number, n=1, and poloidal mode number, $m \sim q_a$ (where q_a is the value of the magnetic winding index, $q = rB_z/RB_\theta$, at the plasma edge) and proposed second-stability experiments will operate with high values of q_a, there exists the possibility that the diamagnetic frequency of the plasma, $\omega_{*i} = -m(c/enBr)dp_i/dr$, may not be negligible when compared to the growth rate, γ, of the ideal mode. When that is the case, the so-called FLR stabilization[33] by ω_{*i} can come into play.

The derivation of the dispersion relation, the relevant boundary conditions and related work can be found in Coppi et al.[34] Considering the simple case of a plasma surrounded by vacuum, the following quadratic form can be constructed from the dispersion equation:

$$\omega^2 - \omega\langle\omega_{*i}\rangle - \langle\omega_0^2\rangle = 0 \tag{1}$$

where to leading order in 1/m:

$$\langle\omega_{*i}\rangle = \frac{\int_0^a dr\ r\omega_{*i}\rho\Lambda^2}{\int_0^a dr\ r\rho\Lambda^2} \tag{2}$$

$$\langle\omega_0^2\rangle = \frac{-a^2\Sigma|\xi_a|^2 + \int_0^a dr\ rF^2\Lambda^2/4\pi}{\int_0^a dr\ r\rho\Lambda^2} \tag{3}$$

$$\Sigma = \frac{B_z^2}{4\pi m R^2 q_a^2}(m - nq_a)$$

$$\times \left[\left(1 + \frac{nq_a}{m}\right) - (m - nq_a)\right] \tag{4}$$

$$F = k \bullet B \quad \text{and} \quad \Lambda^2 = \frac{1}{m^2}|r\xi'|^2 + |\xi|^2. \tag{5}$$

The only term that can produce a growth rate is the boundary term Σ. In particular, we see that $\Sigma > 0$, or equivalently $0 < m - nq_a < 1 + nq_a/m$, is a necessary condition for instability. Conversely, one can show from equation 1 that a sufficient condition for stability is $\min(|\omega_{*i}|) \geq 2\gamma_0$, where γ_0 is the growth rate for $\omega_{*i} = 0$.

---

30 B. Coppi, S. Cowley, R. Kulsrud et al., "High Energy Components and Collective Modes in Thermonuclear Plasmas," *Phys. Fluids* 12: 4060 (1986); G.A. Cottrell et al., "Ion Cyclotron Emission Measurements During JET Deuterium-Tritium Experiments," *Nucl. Fusion* 33: 1365 (1993).

31 B. Coppi, A. Ferreira, J.W.-K. Mark, and J.J. Ramos, "Ideal-MHD Stability of Finite-Beta Plasmas," *Nucl. Fusion* 19: 715 (1979); L. Sugiyama and J.W.-K. Mark, "High-Beta Stability of a Toroidal Plasma," *Phys. Lett. A* 84: 123 (1981).

32 J.J. Ramos, "Tokamak β aB/I Limit and its Dependence on the Safety Factor," *Phys. Rev. A* 42: 1021 (1990); J.J. Ramos, "Complete Macroscopic Stabilization of Tokamak Plasmas," *Phys. Lett. A* 152: 65 (1991).

33 M.N. Rosenbluth, N.A. Krall, and N. Rostoker, "Finite Larmor Radius Stabilization of 'Weakly' Unstable Confined Plasmas," *Nucl. Fusion Suppl.*, Part. 1: 143 (1962).

34 B. Coppi, S. Migliuolo, and B. Rogers, "Removing the Obstacle of External Modes to the Second Stability Region," PTP Report Number 93/8 (Cambridge: MIT Research Laboratory of Electronics, 1993).

In the simplest case of approximately constant ω_{*i}, it is possible to see that ω_{*i} can stabilize the ideal MHD mode by inspection of equation 1. In particular, the dispersion relation $\omega(\omega - \omega_{*i}) = \omega_0^2$ (where ω_0 is the eigenvalue obtained with $\omega_{*i} = 0$) gives

$$\omega = \frac{1}{2}\left(\omega_{*i} \pm \sqrt{\omega_{*i}^2 + 4\omega_0^2}\right) \qquad (6)$$

with the well-known [33] stability condition:

$$\omega_{*i}^2 \geq -4\omega_0^2 \equiv 4\gamma_0^2. \qquad (7)$$

Note that once ω_0 is known, e.g., from a numerical stability analysis[35] of the ideal MHD problem, diamagnetic stabilization can be investigated directly (i.e., without solving the boundary value problem anew) by just evaluating ω_{*i}.

We further specialize our cylindrical analysis to regimes where the ratio of edge to average value of the plasma current, $J_a/\langle J\rangle$, is small and the plasma density (and pressure) do not vanish at the edge. That restricts us to relatively weakly growing ideal modes and benefits the ω_{*i} effect. The relevant dispersion relation, obtained[34] by solving a boundary value problem, is:

$$\omega(\omega - \omega_{*i}) = 3z_0(m - nq_a)^2\omega_{Ap}^2\Delta \qquad (8)$$

where $\omega_{Ap} = B_\theta(a)/(\sqrt{4\pi\rho_a}\, a)$ is the relevant Alfvén transit frequency,

$$\Delta \equiv 1 - \frac{J_a}{(m - nq_a)\langle J\rangle}, \qquad (9)$$

$$z_0 \equiv \frac{(m - nq_a)\langle J\rangle}{\langle J\rangle - J_a}. \qquad (10)$$

It is evident that there is a limit to the ratio $J_a/\langle J\rangle$ for which stability can be attained, but this limit will have to be estimated only after realistic growth rates are obtained from toroidal geometry calculations.

If a perfectly conducting wall is placed at $r = b > a$ surrounding the plasma, the quantity Δ in the dispersion relation (8) is replaced by $\Delta + \Delta_b$, where $\Delta_b = 1/[(b/a)^{2|m|} - 1]$ is positive. Clearly, this can have an important effect in reducing γ_0 to values below the indicated stability threshold.

When finite electrical resistivity of the wall is considered, the two oscillatory modes that arise when the diamagnetic frequency is sufficient to overcome the ideal MHD instability drive (see equation 6), become damped, but a new purely growing mode tends to develop with growth time that is proportional to the resistive diffusion time in the wall. This mode appears to be "immune" to FLR stabilization.

1.3.3 Stabilization of Internal Kinks by Circulating Particles

This work is being done in collaboration with F. Porcelli with the JET Joint Undertaking, Abingdon, U.K.

The topic of linear stabilization of internal kinks by energetic particles has received considerable interest since the observation[36] that sawteeth can be prevented in tokamaks by the application of radiofrequency heating at the cyclotron frequency of a minority population of ions. The explanation[37] of this phenomenon resides in the dynamics of the minority ions which are accelerated to high energies (several MeV in the case of the JET experiments): the ions acquire most of their energy when the turning points in their orbits coincide with the plane of resonance with the wave, $\Omega = \omega$ (here ω is the frequency of the applied RF, while $\Omega(r,\theta)$ is the spatially varying cyclotron frequency of the ions). Thus, ion cyclotron resonance heating (ICRH) preferentially energizes ions that are trapped in the bad curvature region of the tokamak by the magnetic well. When these ions are sufficiently energetic, namely, they have a precession frequency (due to grad-B and magnetic curvature) that is larger than the ideal MHD growth rate of an internal kink, they tend to react in a special manner to the perturbation. Instead of $\mathbf{E} \times \mathbf{B}$ drifting with the rest of the plasma, they react so as to conserve the magnetic

---

[35] J.J. Ramos, "Tokamak β aB/I Limit and its Dependence on the Safety Factor," *Phys. Rev. A* 42: 1021 (1990); J.J. Ramos, "Complete Macroscopic Stabilization of Tokamak Plasmas," *Phys. Lett. A* 152: 65 (1991).

[36] J. Jacquinot et al., "Radiofrequency Heating on JET," The JET Team, in *Plasma Physics and Controlled Nuclear Fusion Research 1986* (Vienna, IAEA: 1987), Vol. I, p. 449.

[37] B. Coppi, R.J. Hastie, S. Migliuolo, F. Pegoraro, and F. Porcelli, "Suppression of Internal Plasma Oscillations by Trapped High Energy Nuclei," *Phys. Lett. A* 132: 267 (1988).

flux contained within the plane defined by the precession of each individual guiding center.[38] An increase in the potential energy of the system ensues, provided certain conditions (e.g., centrally peaked pressure profile) are met.

Here, we dwell anew on the interplay between energetic particles and m=1 internal kinks, concentrating on the circulating species. As is rather obvious, passing particles tend to spend a larger fraction of their time in the region of good curvature ($\theta \sim \pi$ in tokamaks with circular cross-section) and thus their streaming along the field lines tends to negate the radial displacement imposed by the m=1 perturbation. Thus, this population tends to provide a potential energy "hill" that the mode must overcome in order to become unstable. As we show below, the quantitative effect can be of the same order as that provided by the trapped ions discussed in the more standard descriptions.

We remember the dispersion relation for the m=1 internal kink in the ideal limit:

$$\omega(\omega - \omega_{*i}) + \omega_{Ap}^2(\lambda_H + \lambda_k)^2 = 0 \qquad (11)$$

where $\omega_{Ap} = v_A/\sqrt{3}\,R$ is the characteristic Alfvén frequency, $\omega_{*i} = (c/enBr)(dp_i/dr)$ is the ion diamagnetic frequency (computed at $r = r_1$, the position where the magnetic winding index $q(r) = rB_\zeta/RB_\theta$ is equal to unity; here ζ and θ are the toroidal and poloidal coordinates). The quantity λ_H is a measure of the free energy available from the plasma pressure gradient (it is proportional[39] to the square of $\beta_p = (8\pi/B_\theta^2)[\langle p\rangle - p(r_1)]$ where $\langle p\rangle$ is the mean pressure within $r \le r_1$) and must be sufficiently positive for an ideal mode to become unstable in the presence of diamagnetic effects). The term denoted λ_k is the contribution from the energetic particles and is the subject of this discussion. We refer the reader to, e.g., Coppi et al.,[40] for the derivation of this term. Here, we limit ourselves to stating that it is composed of two parts: one, which we term "adiabatic" to which all particles (trapped and circulating) contribute, the other, which we call "non-adiabatic" is due to trapped particles only (under the assumption that the mode frequency is much smaller than the transit frequency of the energetic passing ions). Focus on the contribution from the "adiabatic" portion

$$\lambda_k^{ad} = -\frac{4\pi^2}{R(rq'B_\theta)_{r1}^2}\left(\frac{2}{m_h}\right)^{3/2}\int_0^{r_1} dr\ r$$

$$\int_{-\pi}^{\pi}\frac{d\theta}{2\pi}\cos\theta\int_0^{\varepsilon_M} d\varepsilon\ \varepsilon^{3/2}\int_0^1\frac{d\alpha}{\sqrt{1-\alpha}}$$

$$\times\ (2-\alpha)\frac{\partial F_h}{\partial r} \qquad (12)$$

where ε_M is the maximum energy of this population. When the distribution function of the energetic particles, F_h, is isotropic (function of energy but not magnetic moment, $\mu = mv_\perp^2/B = \alpha\varepsilon/B(r,\theta)$) this term vanishes identically (the $\cos\theta$ factor averages out). Thus, it was found[41] that fusion alpha particles would contribute only via their trapped fraction to the linear stability of internal kinks and would do so through the "non-adiabatic" part of λ_k. As has been indicated in several works (see, e.g., the review articles[42] and references therein) this term is stabilizing ($\lambda_k^{nad} < 0$) for peaked pressure profiles ($dp_h/dr < 0$).

Consider now the case of a population consisting entirely of deeply trapped particles. It can be shown[43] that the stabilizing contribution λ_k is now decreased by a factor $1 - q_0$ (where q_0 is the value of q(r) at the magnetic axis), all other factors being

---

38 F. Porcelli, "Fast Particle Stabilization," *Plasma Phys. Cont. Fusion* 33: 1601 (1991).

39 M.N. Bussac, R. Pellat, D. Edery, and J.L. Soulé, "Internal Kink Modes in Toroidal Plasmas with Circular Cross Sections," *Phys. Rev. Lett.* 35: 1638 (1975).

40 B. Coppi, S. Migliuolo, and F. Porcelli, "Macroscopic Plasma Oscillation Bursts (fishbones) Resulting from High-Energy Populations," *Phys. Fluids* 31: 1630 (1988); B. Coppi, S. Migliuolo, F. Pegoraro, and F. Porcelli, "Global Modes and High Energy Particles in Ignited Plasmas," *Phys. Fluids* B2: 927 (1990).

41 B. Coppi, S. Migliuolo, F. Pegoraro, and F. Porcelli, "Global Modes and High Energy Particles in Ignited Plasmas," *Phys. Fluids* B2: 927 (1990).

42 F. Porcelli, "Fast Particle Stabilization," *Plasma Phys. Cont. Fusion* 33: 1601 (1991); S. Migliuolo, "Theory of Ideal and Resistive M=1 Modes in Tokamaks," *Nucl. Fusion* 33: 1741 (1993).

43 R.J. Hastie, Y. Chen, F. Ke, S. Cai, and L. Chen, "Energetic Particle Stabilization of m = 1 Internal Kink Mode in Tokamaks," *Chin. Phys. Lett.* 4(12): 561 (1987).

equal (i.e., same pressure gradient). Thus, the inference is that the "adiabatic" portion of λ_k provided by trapped particles is positive (destabilizing). As discussed earlier,[44] a trapped particle lives in the bad curvature region, on the average, and will contribute in a destabilizing manner from its fluid-like ("adiabatic") part of the response.

It then stands to reason that the average circulating particle contributes a stabilization to the system by counteracting the fluid-like term due to the trapped particles (i.e., summing circulating and trapped contributions leads to an overall cancellation of the adiabatic piece). Thus, the circulating particles are termed[44] to play a "sacrificial role."

To put this in a more quantitative context, consider the adiabatic contribution anew, writing it as:

$$\lambda_k^{ad} = -\frac{8\pi\sqrt{2}}{(rq'B_\theta)^2_{r_1}} \int_0^{r_1} dr \left(\frac{r}{R}\right)^{3/2}$$

$$\int_0^{\varepsilon_M} d\varepsilon\ \varepsilon^{3/2}(G_T + G_C) \qquad (13)$$

where G_T and G_C are contributions from the trapped and circulating particles, respectively:

$$G_T = \int_0^1 d\kappa\{[2E(\kappa) - K(\kappa)]\}$$

$$\left(\frac{2}{m_h}\right)^{3/2} \frac{\partial F}{\partial r} \qquad (14a)$$

$$G_C = \int_1^{R/r} d\kappa \left\{ \frac{1}{\sqrt{\kappa}} [2\kappa(E(1/\kappa) - K(1/\kappa)) + K(1/\kappa)] \right\}$$

$$\left(\frac{2}{m_h}\right)^{3/2} \frac{\partial F}{\partial r}. \qquad (14b)$$

Here κ is a pitch angle variable (the range $0 \le \kappa \le 1$ corresponds to trapped particles), and K and E the first two complete elliptic integrals. The terms in curly brackets are simply the orbit average of $\cos\theta$ (between turning points $\pm\theta_0$ for trapped particles and between $\pm\pi$ for circulating particles). They are the same factors found in the orbit average of the geodesic portion of the precession frequency, ω_D. The dependence of these terms on pitch angle can be seen, e.g., in figure 9 of Coppi and Rewoldt,[45] (note that our terms correspond to $2K(\kappa)G_1(\kappa)$ in their notation). It is obvious from this figure that circulating particles give a stabilizing contribution ($\lambda_k^{ad} < 0$) for centrally peaked pressure profiles. Note that the contribution is maximal for particles that are near the trapping boundary ($\kappa = 1$) and that barely trapped particles on the other side of the boundary also give a stabilizing contribution via their adiabatic term. The mechanism is the same as for the circulating particles: their orbits have turning points that are near the inner midplane of the torus ($\theta \sim \pi$) and consequently they spend the greater part of their time in the region of good curvature. However, these barely trapped particles (so-called "sloshing" particles[46] will not actually stabilize the mode: unlike the circulating particles (whose entire contribution to the problem is contained within λ_k^{ad}), their response involves the kinetic term, λ_k^{pad}. It turns out that these barely trapped particles are also the ones for which drift reversal has occurred, namely $\omega_{*h}\omega_{Dk}^{(0)} < 0$ (here $\omega_{Dk}^{(0)}$ is the bounce-averaged precession frequency). The drift reversal point is a function of the magnetic shear at the q=1 surface and located between the point where $G_c = 0$ and the trapped-circulating boundary ($\kappa = 1$) for positive shear (cf. figure 9 of Coppi and Rewoldt).[45] Thus, a cancellation between the fluid-like and kinetic contributions to λ_k from these sloshing particles tends to occur. Note also that particles that sit in the very near proximity of the trapped-circulating boundary are subject to scattering (by collisions and/or fluctuations).[47] Thus, most of the stabilization will come from circulating particles located in the region $1 < \kappa \le 2$.

We conclude by noting that the contribution from energetic circulating particles to the problem of m=1

---

[44] F. Porcelli, "Fast Particle Stabilization," *Plasma Phys. Cont. Fusion* 33: 1601 (1991).

[45] B. Coppi and G. Rewoldt, "Collective Modes in Confined High Temperature Plasmas," in *Advances in Plasma Physics,* ed. A. Simon and W. Thompson (New York: Interscience, 1976), Vol. 6, p. 421.

[46] M.N. Rosenbluth, S.T. Tsai, J.W. VanDam, and M.G. Engquist, "Energetic Particle Stabilization of Ballooning Modes in Tokamaks," *Phys. Rev. Lett.* 51: 1967 (1983).

[47] B. Coppi and A. Taroni, "Quasi-Trapped Particle Orbits due to Toroidal Plasma Modes," *Plasma Phys.* 16: 161 (1972).

mode linear stability can be schematically written as:

$$\lambda_k = -\left(\frac{r_1}{R}\right)^{3/2} \frac{\beta_{ph}}{(rq')^2_{r_1}} C \qquad (15)$$

where β_{ph} is the hot particle poloidal beta defined in the same manner as for isotropic distributions (cf. equation (IV-33) of Migliuolo[48]) and C represents the pitch angle contribution, which is of order unity for "slowly passing" particles. This contribution is of the same order as that due to the trapped portion of an isotropic distribution of energetic particles. One is therefore led to propose that sufficiently energetic neutral beams, injected tangentially to the magnetic field, may be effective in producing sawtooth-free discharges in tokamaks.

1.3.4 Deuterium-Helium(3) Fusion Burning Using ICRH Minority Heating in Ignitor

The design characteristics of the Ignitor experiment[49] allow it to satisfy the conditions where the 14.7 MeV protons and the 3.6 MeV α-particles produced by the D-^{3}He reactions can supply thermal energy to a well confined plasma. In particular, Ignitor:

- can sustain a plasma current exceeding that required ($I_p \geq 6$MA) to confine the proton orbits at birth;
- can produce sufficiently high plasma densities that the slowing down time of both the protons and the α-particles is shorter than the electron energy replacement time of the thermal plasma in which they are generated.

In order to boost the D-^{3}He fusion reaction rate, ion-cyclotron heating of a D plasma with a ^{3}He minority can be used to create a tail in velocity space for the ^{3}He distribution function[50] with an optimal mean energy value. We note that the D-^{3}He fusion cross section has a maximum near $E \simeq 650$ keV for a helium beam incident on a deuterium target.

A preliminary analysis of the fusion power P_F that may be produced in Ignitor by this method indicates that $P_F \simeq 1$ MW may be reached, thanks primarily to the high value of the RF power density that can be coupled to the helium nuclei. We recall that in previous experiments, fusion power levels of 1.5 kW and 140 kW have been obtained in PLT[51] and in JET[52] respectively. However, neither of these experiments had the current and particle densities required for the confinement and the slowing-down of the 14.7 MeV protons.

Numerical simulations for this scenario in Ignitor were performed using the FPPRF[53] code, that combines a ray tracing package with the solution of the Fokker-Planck equation for the minority species. Typical RF parameters were $P_{RF} = 18$ MW, $\nu = 132$ MHz, $\langle k_\parallel \rangle = 5 - 10\ m^{-1}$. The parallel wavelength $\langle k_\parallel \rangle$ is estimated on the basis of the size of the adopted ICRH antennas. The ray tracing routine (SPRUCE) solves the dispersion relation for electromagnetic waves propagating in a hot plasma, while another set of routines evolves the distribution function of the minority ions in time by solving the bounce-averaged Fokker-Planck equation:

$$\frac{\partial f}{\partial t} = \langle Q \rangle + \langle C \rangle + \langle S \rangle \qquad (16)$$

where <Q> represents the power deposition by the wave and is a quasilinear operator which computes the (spatially varying) resonant wave-particle energy exchange, <C> is the standard collision operator involving pitch angle scattering, slowing down (by electrons and background ions) and energy exchange with other species (electrons and ions), and <S> represents the combination of sources and sinks (charge exchange, prompt losses of fast ions, etc.).

---

48 S. Migliuolo, "Theory of Ideal and Resistive M=1 Modes in Tokamaks," *Nucl. Fusion* 33: 1741 (1993).

49 B. Coppi, M. Nassi, and L.E. Sugiyama, "Physics Basis for Compact Ignition Experiments," *Phys. Scripta* 45: 112 (1992).

50 T.H. Stix, "Fast Wave Heating of a Two-Component Plasma," *Nucl. Fusion* 15: 737 (1975).

51 R.E. Chrien and J.D. Strachan, "D-^{3}He Reaction Measurements during Fast Wave Minority Heating in the PLT Tokamak Experiment," *Phys. Fluids* 26: 1953 (1983).

52 J. Jaquinot, G.J. Sadler, and the JET Team, "D-^{3}He Fusion in the Joint European Torus Tokamak: Recent Experimental Results," *Fusion Technol.* 21: 2254 (1992).

53 G.W. Hammett, *Fast Ion Studies of Ion Cyclotron Heating in the PLT Tokamak,* Ph.D. diss., Princeton University, 1986.

The code returns wave dispersion properties (in particular $N_\perp^2(r)$, where $\vec{N} = \vec{kc}/\omega$ is the index of refraction), the RF power deposition profile as a function of r and θ, the minority ion distribution function $f(r,E,\mu)$, the mean energy of the RF heated minority as a function of r, as well as an estimate of the beam-target fusion reaction yield (i.e., number of protons per second, for the case of D-^{3}He where the "beam" is composed of ^{3}He ions and the "target" of D ions). The code is able to treat the interaction with the minority species at either the fundamental or the first harmonic of the cyclotron frequency.

In the minority heating scenario for the fast wave, four characteristic distances can be identified that are important for the damping of the wave. in terms of $x = R - R_{mag}$, (where $R_{mag} \simeq R_o$ is the distance of the magnetic axis from the symmetry axis), these are:

1. $x_c = 0$, the distance of the cyclotron resonance $\omega = \Omega_{He}$ of the helium ions (note that the wave field at this location has mostly a right-handed polarization which is opposite to the one required for optimal coupling with the ion gyromotion);

2. $\Delta x_c = k_\parallel V_{th,He}/\omega R_{mag}$, the width of the thermal broadening of the cyclotron resonance;

3. $x_L \simeq -(1/2)(n_{^3He}/n_e)R_{mag}$, the distance of $N_\parallel^2 = L \simeq \Sigma_i(\omega_{pi}/\Omega_{ci})^2\Omega_{ci}/(\Omega_{ci} - \omega)$ cut-off surface $k_\perp^2 = 0$ (the other cut-off surface, $N_\parallel^2 = R \simeq \Sigma_i(\omega_{pi}/\Omega_{ci})^2\Omega_{ci}/(\Omega_{ci} + \omega)$, is located near the plasma periphery). In the cold plasma approximation, at x_L the wave has a complete left-hand polarization;

4. $x_S \simeq -(7/12)(n_{^3He}/n_e)R_{mag}$, the distance of $N_\parallel^2 = S \equiv (R + L)/2$ ion hybrid resonance surface $k_\perp^2 \to \infty$. When the effects of finite plasma temperature are taken into account, the (electromagnetic) fast wave can couple to the (electrostatic, short wavelength) ion Bernstein wave (mode conversion) near the ion hybrid surface leading to heating of the bulk plasma.

When ICRH is applied in the minority heating regime it is important that:

1. the evanescent region separating the cutoff and ion hybrid resonance surfaces be as large as possible in order to minimize direct heating of the bulk plasma via mode conversion (we find that the addition of a small concentration of a third ion species—hydrogen or tritium—is helpful in this respect);

2. the width $|\Delta x_c|$ be broad enough to overlap the cutoff surface where optimal conditions of wave field polarization for coupling with helium gyromotion are encountered.

As the helium is heated from the initial plasma temperature to an effective tail temperature of 1 MeV (or more), the width $|\Delta x_c|$ is seen to increase from 0.01 m to 0.1 m, finally overlapping the cutoff region. Accordingly the peak in $Im(N_\perp)$, associated with the damping of the wave, moves from its original position at the cyclotron resonance toward the $N_\parallel^2 = L$ cutoff surface.

The helium distribution function is obtained, at several times during the simulation, and the relevant level lines in the $(v_\parallel, v_\perp)$ plane, show the characteristic[54] two-horn shape with values of the pitch angle about 60-80 degrees. Analytically, f can be described by a combination of a core Maxwellian and an anisotropic tail with a characteristic perpendicular mean energy[55] given by $T_{eff} = T_e[1 + (3/2)\xi_{RF}]$. Here $\xi_{RF} \simeq \rho_{RF}\tau_s/(3n_{He}T_e)$, while τ_s is the slowing down time of the helium nuclei and ρ_{RF} the local value of RF power density coupled to them. Therefore,

$$\xi_{RF} = \frac{\hat{T}_e^{1/2}}{\hat{n}_e \hat{n}_{He} \ln \hat{\Lambda}} \left(\frac{<\rho_{RF}>}{MW/m^3} \right) \qquad (17)$$

when written in practical units ($\hat{T} = T/10$ keV, $\hat{n} = n/10^{20}\,m^{-3}$, $\ln \hat{\Lambda} = \ln \Lambda/10$). Generally, over 95 percent of the RF power is deposited (promptly) into the helium. A substantial fraction of this power (up to 50 percent) is then transferred to the electrons by collisional processes. The fusion power output is estimated with several simplifying assumptions (e.g., an isotropic velocity distribution function for the fast ions) and the quoted value $P_F \simeq 1$ MW should be considered as preliminary.

Alternatively, we have also computed the D-^{3}He reactivity parameter $<\sigma v>_F$ for a ^{3}He distribution function as given by Stix.[55] The relevant two-dimensional velocity space integral is computed

---

[54] G.W. Hammett, *Fast Ion Studies of Ion Cyclotron Heating in the PLT Tokamak,* Ph.D. diss. (Princeton, New Jersey: Princeton University, 1986).

[55] T.H. Stix, "Fast Wave Heating of a Two-Component Plasma," *Nucl. Fusion* 15: 737 (1975).

numerically. For a given set of temperatures, there is an optimal value of ξ_{RF} for which $\langle\sigma v\rangle_F$ is maximum, and this value can be lowered considerably by increasing T_e and T_i. Since ξ_{RF} is inversely proportional to the square of the electron density (for constant minority concentration), while $P_F \propto n_{He} n_D \langle\sigma v\rangle_F$, an increase in the bulk plasma temperature allows a higher optimal density at constant values of ρ_{RF} and therefore of P_F.

A zero-dimensional (no quantitative radial profile effect included) estimate of the total fusion power can be obtained from $\langle\sigma v\rangle_F$ in the following way. On the basis of the inferred value of $\langle\rho_{RF}\rangle$, we can select, for given temperatures, an optimal density product $\hat{n}_e \hat{n}_{He}$. This is determined in such a way that the corresponding value of ξ_{RF} is the one for which $\langle\sigma v\rangle_F$ is maximum, i.e., $\langle\sigma v\rangle_F^{max} \simeq 2.0 \times 10^{-22}$ m²/s. Then assuming that these optimal conditions can be produced only in a small fraction V_{eff} of the total plasma volume (say $V_{eff} \simeq (1/25)$ V), we estimate

$$P_F \simeq 6(\hat{n}_D \hat{n}_{He})^{optimal} \times (V_{eff}/m^3)MW \quad (18)$$

In the case where $T_e = 20$ keV, $T_i = 15$ keV for example, and $\langle\rho_{RF}\rangle = 65$ MW/m³ over V_{eff}, we find $\hat{n}_e^{optimal} \simeq 2.5$ and $\hat{n}_{He}^{optimal} \simeq 0.2$, so that $P_F \simeq 1$MW. This value is in reasonable agreement with that obtained from the code FPPRF under similar conditions.

1.3.5 Deuterium-Tritium Ignition Experiments with High Magnetic Fields

High magnetic field experiments have been designed to investigate deuterium-tritium fusion ignition conditions, on the basis of known experimental and theoretical understanding of plasma behavior. Our group has long maintained a strong effort in pioneering the practical use of such configurations. We have shown that the most advantageous and least expensive designs incorporate an interlocking set of characteristics[56] —tight aspect ratio, relatively small size with significant vertical elongation, high toroidal and poloidal magnetic fields, large plasma currents, high plasma densities, good plasma purity, strong ohmic heating, good plasma and α-particle confinement, and robustness against ideal MHD and resistive plasma instabilities. We have investigated the physical basis for these plasma properties, while also constructing the design and engineering solutions for attaining the necessary parameters (in the Ignitor Ult machine[56] presently being built in Italy). Since ignition depends upon many spatially and temporally varying processes, many of our studies are based upon the numerical simulation of a free boundary plasma from the current ramp through ignition, using the MHD evolution and plasma flux surface transport code, TSC.[57]

The ignition of a 50:50 deuterium-tritium plasma requires a minimum value of the parameter $n_o \tau_E \simeq 4 \times 10^{20}$ sec/m³ in order to achieve ignition with $T_{eo} \simeq T_{io} \leq 15$ keV, where n_o is the peak plasma (electron) density, T_{eo} the peak temperature, and τ_E the energy replacement time. Here ignition is defined to be the point when the plasma heating due to fusion α-particles, P_α, equals the plasma thermal losses P_L. Relatively high values of the plasma density, $n_o \simeq 10^{21}$ m⁻³, then require only moderate values of τ_E, whose magnitude is less easy to predict with certainty. Both these values should be achievable, based on the favorable confinement properties of high density plasmas that have been demonstrated by a series of high field experiments, the Alcator A and C and the latest, the Alcator CMOD, at MIT and the FT/FTU devices at Frascati, Italy. Experimentally, the maximum plasma density n_o that can be supported correlates with the ratio B_T/R_o, where B_T is the toroidal magnetic field at the center of the plasma column, at major radius $R = R_o$. On the basis of the Alcator C machine, where $n_o \simeq 2 \times 10^{21}$ m⁻³ was achieved with $B_T \simeq 12.5$ T and $R_o = 0.64$ m, and the TFTR machine at Princeton, where even larger ratios of $n_o R_o/B_T$ were achieved, a configuration with $R_o \simeq 1.3$ m and $B_T \simeq 13$ T should be able to sustain reliably densities of 10^{21} m⁻³.

A strong toroidal magnetic field also supports a high poloidal field B_p and correspondingly large plasma current I_p. A significant vertical elongation, e.g., $\kappa \simeq 1.8$, substantially increases the plasma current that can be carried for a given B_T and R. If the density correlates with the (volume) averaged toroidal current density, $\langle J_\phi \rangle$, then experimental results suggest that somewhat less than 1kA/cm² should offer considerable margin to attain the desired peak density $n_o \sim 10^{21}$ m⁻³. High values of B_p produce a strong rate of ohmic heating, while large currents I_p tightly confine the fast α-particles produced by the fusion reactions, so that they deposit their energy in the center of the plasma.

---

[56] B. Coppi, M. Nassi, and L.E. Sugiyama, "Physics Basis for Compact Ignition Experiments," *Phys. Scripta* 45: 112 (1992).

[57] S.C. Jardin, N. Pomphrey, and J. Delucia, "Dynamic Modelling of Transport and Positional Control of Tokamaks," *J. Comp. Phys.* 66: 481 (1986).

The degradation of the plasma energy confinement, commonly observed when injected (nonohmic) heating is applied, is reduced at higher plasma current. In addition, the poloidal plasma beta β_p can be kept small at ignition to improve the plasma stability and in particular to stabilize the ideal MHD modes with mode numbers m=1, n=1 that are associated with sawtooth oscillations. Large plasma density combined with good ohmic heating allows ignition at low plasma temperatures. This reduces the fusion power, and therefore the thermal wall loads. The low beta increases the overall margin of plasma stability.

The plasma purity has been shown to improve with increasing plasma density, that is, the effective charge $Z_{eff} = \sum n_i Z_f^2/n_e$ decreases monotonically with n_e, in an extensive series of experiments starting with the Alcator A. The major effect of impurities is to dilute the concentration of fusing nuclei, while a secondary effect is the increase of power loss due to bremsstrahlung radiation. If auxiliary heating is not used, Z_{eff} cannot exceed about 1.6 for D-T ignition in the Ignitor, as indicated by our analyses.

Relatively high plasma edge densities also help to confine impurities to the scrape off layer, where the induced radiation helps to distribute the thermal wall loading more uniformly over the plasma chamber surface. The low ignition temperatures associated with high density further help to keep the plasma clean, by reducing the thermal wall loading, that result in sputtering.

Peaked plasma density profiles should be maintained, by external means such as pellet injectors, if necessary. Peaked profiles maintain stability to ion temperature gradient modes that enhance the ion thermal transport. Since the neoclassical (Ware) inward particle pinch is relatively strong in a tight aspect ratio, high field configuration and an anomalous inflow is also present, pellets that penetrate partway into the plasma can be successfully used to raise the plasma density and produce peaked profiles near ignition.

Plasma configurations, such as X-points, that concentrate the thermal (particle) heat flux on localized areas of the vessel wall, limit the amount of fusion power that can be handled. In addition, a more limited plasma current can be sustained. However, X-points and detached plasmas can be obtained with relatively little sacrifice in the plasma and magnet parameters and they may prove desirable to limit the degradation of the plasma confinement caused by nonohmic heating, by creating the conditions known to produce "H-mode" operation.

Divertors represent a more severe compromise, since they alter the design of the plasma chamber and the toroidal magnet. The major radius must be increased to accomodate a reliable divertor, reducing the ratio B_T/R and therefore the maximum plasma density. The magnetic fields are also reduced, lowering the plasma current and the ohmic heating, and increasing β. A large injected heating system becomes necessary to replace the ohmic heating and the resulting degradation of the plasma confinement makes low temperature ignition difficult. The divertor plates must then handle large thermal heat fluxes. There is no demonstrated advantage to using divertors in high density plasmas.

1.3.6 Time Dependent Ignition

The transient nature of ignition has important consequences. The initial current ramp, when I_p, n_e, B_T, and the plasma cross section are increased simultaneously, to their maximum values, has important effects on the plasma energy balance and stability at ignition.[58] These effects arise from the relatively slow inward diffusion of the plasma current, which is added at the outer surface of the plasma by the current ramp, compared to the growth of the central temperature due to plasma heating. The current ramp generates a inhomogeneous toroidal electric field in the plasma that is peaked near the plasma edge and allows large values of ohmic heating at high central temperature. The magnetic safety factor q can be easily maintained above unity or held to a very small $q < 1$ region during the current ramp, and a more careful study,[58] shows that it can also be kept small after the ramp, at least until the central temperature reaches high values and fusion α-particles begin to appear, both of which are stabilizing effects for m=1 modes. Furthermore, small amounts of injected heating (e.g., $P_{INJ} < P_{OH}/2$) during the current ramp can maintain a very small size (or nonexistence) for the $q < 1$ region until well past ignition, if central temperatures approach 10 keV by the end of the current ramp, through the freezing-in of the central current density at low resistivity. Injected heating also reduces the magnetic flux consumption required to reach ignition, particularly if ignition occurs during the current

[58] B. Coppi, M. Nassi, and L.E. Sugiyama, "Physics Basis for Compact Ignition Experiments," *Phys. Scripta* 45: 112 (1992); L. Sugiyama and M. Nassi, "Free Boundary Current Ramp and Current Profile Control in a D-T Experiment," *Nucl. Fusion* 32: 387 (1992).

ramp. These characteristics are illustrated in table 3 (reference case for the maximum Ignitor design parameters, peak B_T = 13.5 T, I_p = 12 MA, R = 1.3 m, a = 0.48 m, κ = 1.8, and $n_{eo} = 1.1 \times 10^{21}$ m^{-3}, at 50:50 D:T ratio and Z_{eff} = 1.2).

It has been shown that it is simultaneously possible to maintain monotonically increasing q profiles without large low shear regions, and with edge values $3 < q_{\psi a} < 4$ during the current ramp, to beyond ignition. These conditions should prevent instabilities associated with internal plasma modes (e.g., "locked" or quasistationary modes) that can be triggered during the current ramp and often lead to serious disruptions, in which the confinement of the plasma can be lost. Since hollow q profiles are usually associated with the excitation of internal macroscopic modes and enhanced, "anomalous" current penetration, while ignition is aided by a slow current penetration that keeps $q_o > 1$ for as long as possible, these precautions are not superfluous.

A major question for all ignition experiments is the degree of degradation expected in the plasma energy confinement near ignition, since D-T ignition is easily achieved if the confinement remains at the optimal, ohmic heating level. One strategy for a high field experiment is to maintain a high level of ohmic heating up to ignition, $P_\alpha \leq 2P_{OH}$, to reduce the degree of degradation. Since α-particle heating possesses two important characteristics of ohmic heating that are not shared by any presently available form of injected heating—axisymmetric deposition and generation in the center of the plasma column—we expect that the degradation should not be as severe.

Table 3. Reference Discharge for the Ignitor Ult Maximum parameters at the End of Ramp I_p = 12 MA, B_T = 13.5 T, R = 1.3 m, a = 0.48 m, b = 0.87 m, $\delta \sim 0.4$, $n_{eo} = 1.1 \times 10^{21}$ m^{-3}, $n_{eo}/\langle n_e \rangle = 2.2$, $Z_{eff} = 1.2$.

	End Ramp	Ignition	
t	3.0	4.3	time (sec)
$\ell_i/2$	0.32	0.38	internal inductance
β_p	0.08	0.13	poloidal beta
β	0.8	1.26	toroidal beta (%)
$q_{\psi a}$	3.3	3.6	edge magnetic safety factor
W	7.5	11.7	plasma kinetic energy (MJ)
T_{eo}	4.0	11.0	peak electron temperature (keV)
τ_E	710	660	energy confinement time (msec)
P_{OH}	13.0	9.5	ohmic heating (MW)
P_α	2.0	17.8	α-particle heating (MW)
$n_{\alpha o}$	1.5	12.0	peak α-particle density (10^{17}m^{-3})
P_B	3.2	4.1	bremsstrahlung radiation (MW)
P_{IC}	0.4	0.5	cyclotron and impurity radiation (MW)
$V_{q=1}$	1.4	5.8	volume where $q \leq 1$ (% of total)
$\Delta\Phi$	29.2	31.4	magnetic flux variation (V sec)
I_{BS}	0.6	1.0	bootstrap current (MA)

The requirement that the edge q is between 3 and 4 (high plasma current) means that special care must be devoted to maintaining $q > 1$ up to ignition. If only ohmic heating is contemplated, the steadily increasing size of the $q < 1$ region after the end of the current ramp imposes a more severe limit on the time in which the plasma can ignite and on the required energy confinement level, than the

energy balance alone, if it is assumed that sawtooth oscillations large enough to destroy the central peaking of the temperature cannot be avoided. Then ignition in the Ignitor reference case, at $T_o \simeq 11$ keV, requires $\tau_E \simeq 0.66$ sec and must occur within approximately 1.5 sec of the end of the current ramp (table 1). Our theoretical analysis, on the other hand, indicates that Ignitor remains, in all regimes, within the stability limits of the ideal MHD and resistive m=1, n=1 modes. In addition, moderate amounts of auxiliary heating, $P_{ICRH} \sim 10 - 15$ MW, started during the current ramp, allow ignition down to the limits predicted by $n_o\tau_E$, i.e., $\tau_E \leq 0.4$ sec, while maintaining very small q=1 regions well beyond ignition. Similarly, in the ohmic case, if the requirement of small $q < 1$ region is dropped, either on the basis of the theoretical analysis or by externally stabilizing the sawtooth oscillations, ignition can also occur at these τ_E's and times of $t_I \simeq 5 - 5.5$ sec.

The importance of ohmic heating during the ignition sequence at high field and density means that a model for the electron thermal transport should, like the one used here, simulate ohmic regimes and reproduce typical toroidal loop voltages in steady state ohmic experiments, that are observed to be an almost "universal" constant. In addition, the total diffusion coefficient should increase with injected heating and reproduce the degraded confinement observed in present experiments that are dominated by injected heating.

A second major question for ignition is the effect of variation in the plasma density and its profile, since pellets injected to raise the density are unlikely to fully penetrate a high density plasma. For a given level of thermal transport, there is an optimum density for fastest ignition. A higher density is more favorable under degraded conditions. Higher density, however, accelerates the toroidal current penetration at a given time by lowering the T_e, producing larger $q < 1$ regions earlier than at lower density. This effect also operates in the outer part of the plasma radius when density profiles are broadened. Thus, for $n_{eo} = 1.1 \times 10^{21}$ m^{-3}, profile peaking factors $n_{eo}/\langle n_e \rangle \geq 1.9$ where $\langle n_e \rangle$ is the volume average give relatively results similiar to the standard case ($n_o = 2 \times 10^{21}$ m^{-3}) for ignition. Broader profiles rapidly lead to degraded ignition, e.g., $n_{eo}/\langle n_e \rangle = 1.5$ requires longer t_I and higher τ_E, and yields a significantly larger q=1 radius. Lower central density, e.g., $n_{eo} = 6.5 \times 10^{20}$ m^{-3} at the end of the current ramp increasing to $8 - 9 \times 10^{20}$ by ignition, allows broader profiles, $n_{eo}/\langle n_e \rangle = 1.5$. For related reasons, increasing the plasma density after the current ramp is more advantageous than increasing the density during the ramp. At high density, a region of low magnetic shear develops in the mid-region of the minor radius. This region becomes seriously unstable when its value of q approaches unity, since ideal MHD instabilities with m=1 can occur. This is one of the major limits on the broad density profile cases.